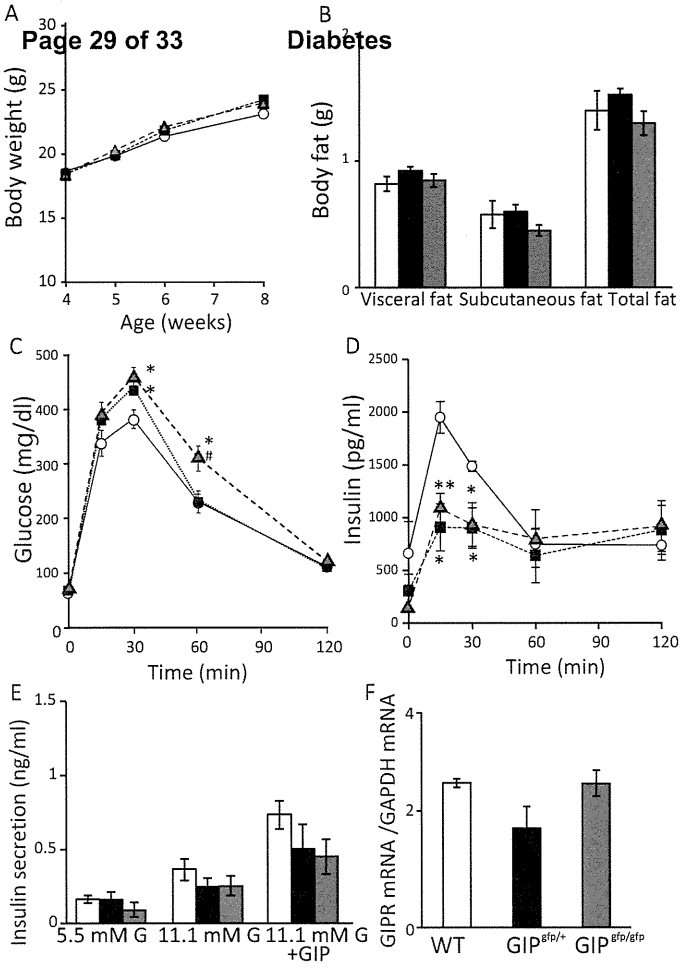
A
Body weight (g)
Age (weeks)
B
Body fat (g)
Visceral fat
Subcutaneous fat
Total fat
C
Glucose (mg/dl)
Time (min)
D
Insulin (pg/ml)
Time (min)
E
Insulin secretion (ng/ml)
5.5 mM G
11.1 mM G
11.1 mM G +GIP
F
GIPR mRNA /GAPDH mRNA
WT
GIP gfp/+
GIP gfp/gfp

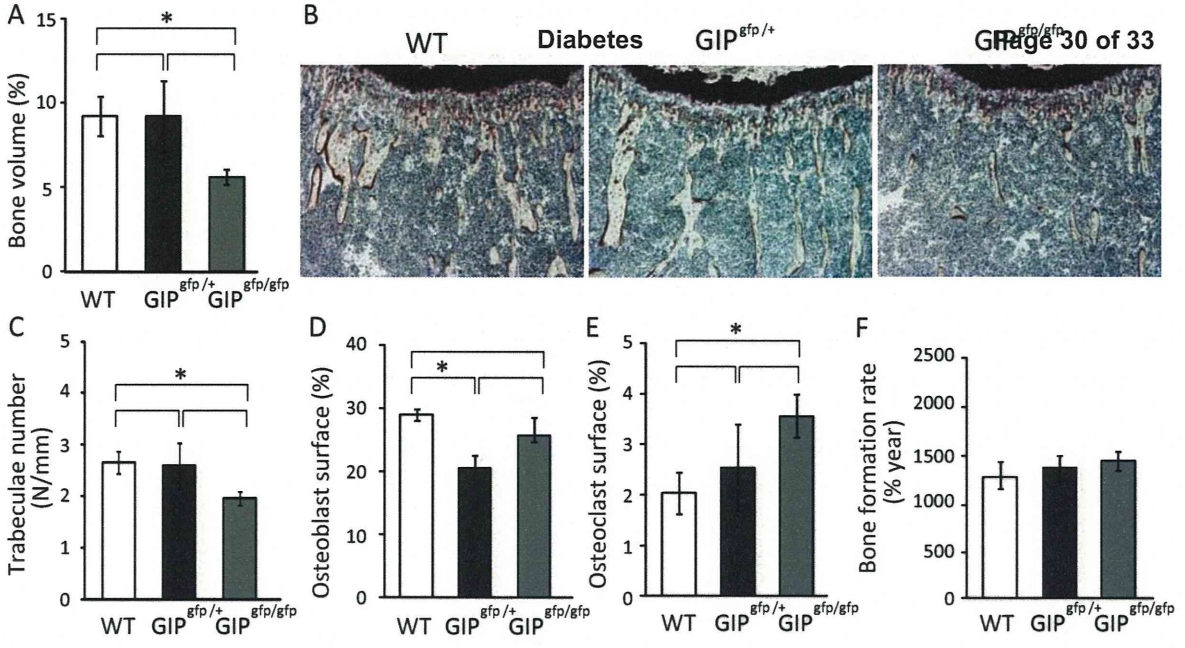
A
Bone volume (%)
15
10
5
0
*
WT
GIP gfp/+
GIP gfp/gfp
B
WT
Diabetes
GIP gfp/+
GIP gfp/gfp
C
Trabeculae number (N/mm)
5
4
3
2
1
0
*
WT
GIP gfp/+
GIP gfp/gfp
D
Osteoblast surface (%)
40
30
20
10
0
*
WT
GIP gfp/+
GIP gfp/gfp
E
Osteoclast surface (%)
5
4
3
2
1
0
*
WT
GIP gfp/+
GIP gfp/gfp
F
Bone formation rate (% year)
2500
2000
1500
1000
500
0
WT
GIP gfp/+
GIP gfp/gfp

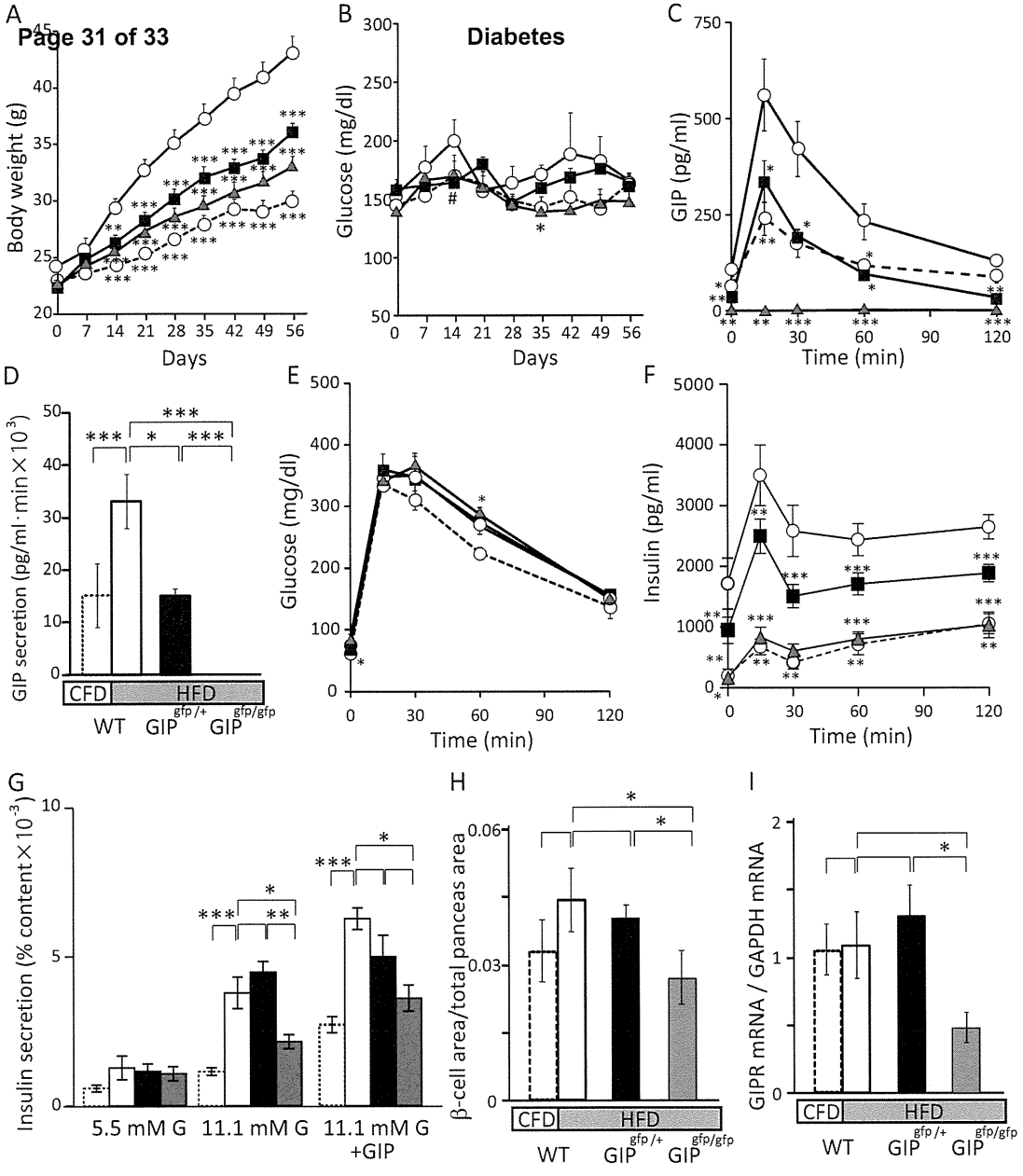
A
Body weight (g)
Days
B
Diabetes
Glucose (mg/dl)
Days
C
GIP (pg/ml)
Time (min)
D
GIP secretion (pg/ml·min×10-3)
CFD
HFD
WT
GIP gfp/+
GIP gfp/gfp
E
Glucose (mg/dl)
Time (min)
F
Insulin (pg/ml)
Time (min)
G
Insulin secretion (% content×10-3)
5.5 mM G
11.1 mM G
11.1 mM G +GIP
H
β-cell area/total panceas area
CFD
HFD
WT
GIP gfp/+
GIP gfp/gfp
I
GIPR mRNA / GAPDH mRNA
CFD
HFD
WT
GIP gfp/+
GIP gfp/gfp

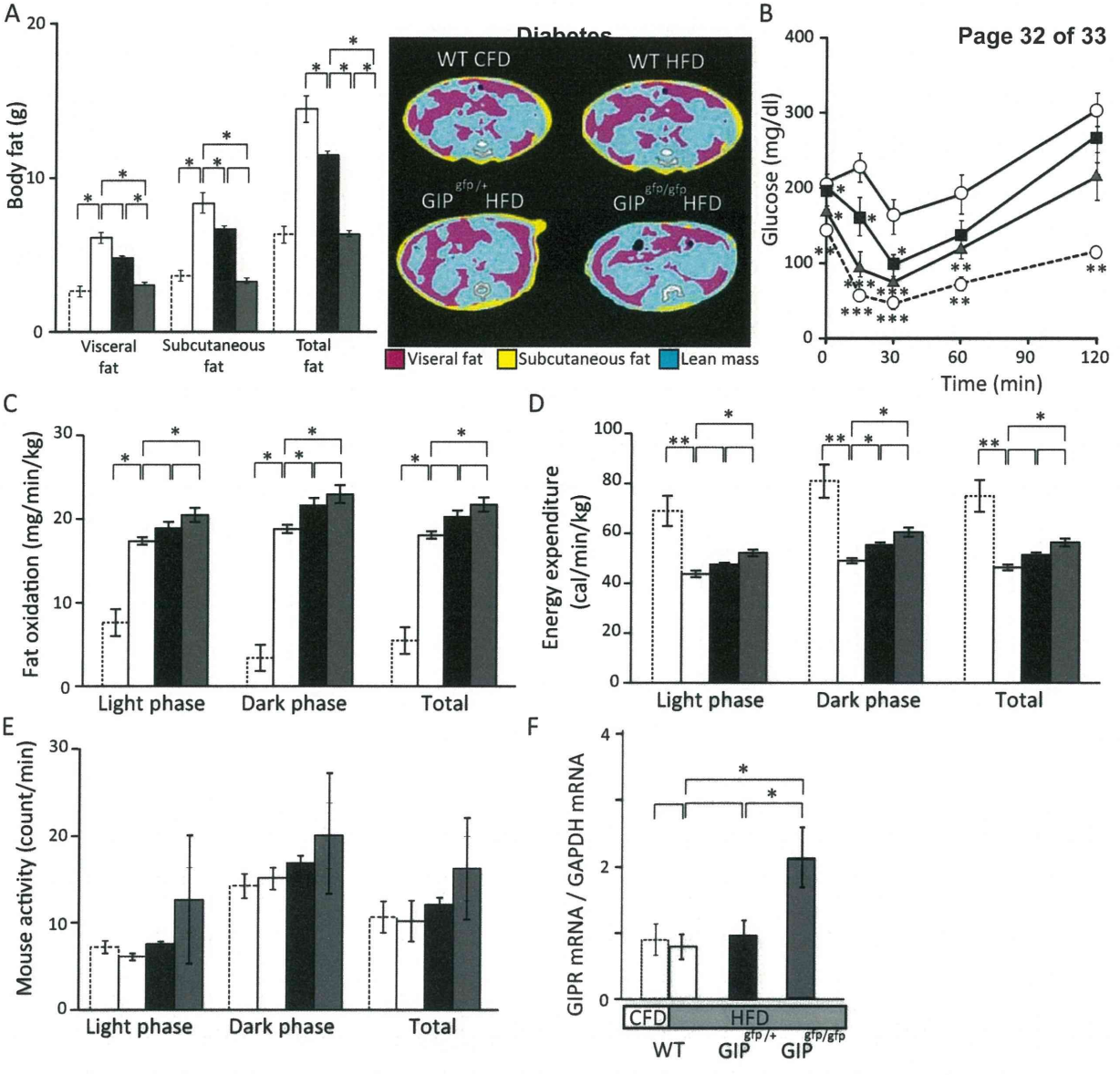
A
Body fat (g)
Visceral fat
Subcutaneous fat
Total fat
WT CFD
WT HFD
GIP gfp/+ HFD
GIP gfp/gfp HFD
Viseral fat
Subcutaneous fat
Lean mass
B
Glucose (mg/dl)
Time (min)
C
Fat oxidation (mg/min/kg)
Light phase
Dark phase
Total
D
Energy expenditure (cal/min/kg)
Light phase
Dark phase
Total
E
Mouse activity (count/min)
Light phase
Dark phase
Total
F
GIPR mRNA / GAPDH mRNA
CFD
HFD
WT
GIP gfp/+
GIP gfp/gfp

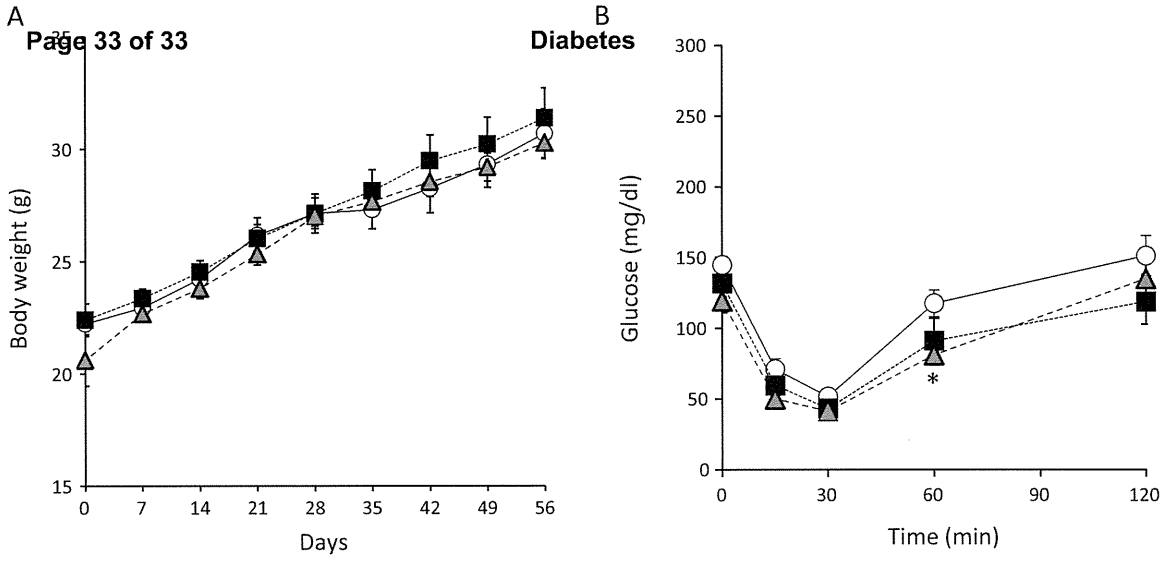
A
Body weight (g)
Days
0
7
14
21
28
35
42
49
56
15
20
25
30
B
Diabetes
Glucose (mg/dl)
Time (min)
0
30
60
90
120
50
100
150
200
250
300
*

Published April 21, 2014

BARP suppresses voltage-gated calcium channel activity and Ca^{2+}-evoked exocytosis

Pascal Béguin,[1,5] Kazuaki Nagashima,[3] Ramasubbu N. Mahalakshmi,[1] Réjan Vigot,[5] Atsuko Matsunaga,[5] Takafumi Miki,[4] Mei Yong Ng,[1] Yu Jin Alvin Ng,[1] Chiaw Hwee Lim,[1] Hock Soon Tay,[2] Le-Ann Hwang,[2] Dmitri Firsov,[6] Bor Luen Tang,[7] Nobuya Inagaki,[3] Yasuo Mori,[4] Susumu Seino,[9] Thomas Launey,[5] and Walter Hunziker[1,8]

[1]Epithelial Cell Biology Laboratory and [2]Monoclonal Antibody Unit, Institute of Molecular and Cell Biology, Agency for Science, Technology and Research, Singapore 138673
[3]Department of Diabetes and Clinical Nutrition, Graduate School of Medicine; and [4]Department of Synthetic Chemistry and Biological Chemistry, Graduate School of Engineering; Kyoto University, Sakyo-ku, Kyoto 606-8501, Japan
[5]Launey Research Unit for Molecular Neurocybernetics, RIKEN Brain Science Institute, Wako-shi, Saitama 351-0198, Japan
[6]Pharmacology and Toxicology Department, University of Lausanne, 1005 Lausanne, Switzerland
[7]Department of Biochemistry and [8]Department of Physiology, Yong Loo Lin School of Medicine, National University of Singapore, Singapore 117599
[9]Division of Cellular and Molecular Medicine, Kobe University Graduate School of Medicine, Chuo-ku, Kobe 650-0047, Japan

Voltage-gated calcium channels (VGCCs) are key regulators of cell signaling and Ca^{2+}-dependent release of neurotransmitters and hormones. Understanding the mechanisms that inactivate VGCCs to prevent intracellular Ca^{2+} overload and govern their specific subcellular localization is of critical importance. We report the identification and functional characterization of VGCC β-anchoring and -regulatory protein (BARP), a previously uncharacterized integral membrane glycoprotein expressed in neuroendocrine cells and neurons. BARP interacts via two cytosolic domains (I and II) with all $Ca_v\beta$ subunit isoforms, affecting their subcellular localization and suppressing VGCC activity. Domain I interacts at the α_1 interaction domain–binding pocket in $Ca_v\beta$ and interferes with the association between $Ca_v\beta$ and $Ca_v\alpha1$. In the absence of domain I binding, BARP can form a ternary complex with $Ca_v\alpha1$ and $Ca_v\beta$ via domain II. BARP does not affect cell surface expression of $Ca_v\alpha1$ but inhibits Ca^{2+} channel activity at the plasma membrane, resulting in the inhibition of Ca^{2+}-evoked exocytosis. Thus, BARP can modulate the localization of $Ca_v\beta$ and its association with the $Ca_v\alpha1$ subunit to negatively regulate VGCC activity.

Introduction

Exocytosis in response to action potential–evoked membrane depolarization has been extensively characterized in the nervous system, in which neurotransmitters or hormones are released after extracellular Ca^{2+} influx at synapses in neurons or in neuroendocrine cells, respectively. In pancreatic islet β cells, for example, glucose elevation results in the closure of K_{ATP} channels, membrane depolarization, opening of voltage-gated calcium channels (VGCCs), and, in response to Ca^{2+} influx, secretion of insulin (Yang and Berggren, 2006). At neuronal synapses, neurotransmitter-containing vesicles are docked in close vicinity to VGCCs at the presynaptic active zone (Neher, 1998; Zhai and Bellen, 2004; Atwood, 2006). Although the spatial proximity of VGCCs and exocytic vesicles undergoing fusion with the plasma membrane is well documented, the detailed molecular mechanisms involved in the spatial and temporal coupling of exocytosis and VGCC activation and inactivation remain to be elucidated.

VGCCs are composed of an ion pore–forming $Ca_v\alpha1$ subunit associated with several auxiliary subunits ($Ca_v\beta$, $Ca_v\alpha2\delta$, and $Ca_v\gamma$; Arikkath and Campbell, 2003). Among the $Ca_v\alpha1$ subunits, the P/Q-type $Ca_v2.1$ and the N-type $Ca_v2.2$ define the main channel subtypes important for presynaptic neurotransmitter release (Spafford and Zamponi, 2003; Evans and Zamponi, 2006), and the L-type $Ca_v1.2$ subtype triggers Ca^{2+}-dependent secretion in neuroendocrine cells (Catterall, 2000). Four $Ca_v\beta$ subunit isoforms

Correspondence to Walter Hunziker: hunziker@imcb.a-star.edu.sg; or Thomas Launey: Thomas.launey@riken.jp

Abbreviations used in this paper: Ab, antibody; ABP, AID-binding pocket; AID, α1 interaction domain; BARP, β-anchoring and -regulatory protein; BDNF, brain-derived neurotrophic factor; GFAP, glial fibrillary acidic protein; hGH, human growth hormone; PSS, physiological salt solution; VGCC, voltage-gated calcium channel; WB, Western blot; WT, wild type.

Supplemental Material can be found at:
http://jcb.rupress.org/content/suppl/2014/04/17/jcb.201304101.DC1.html

The Rockefeller University Press $30.00
J. Cell Biol. Vol. 205 No. 2 233–249
www.jcb.org/cgi/doi/10.1083/jcb.201304101

Published April 21, 2014

($Ca_v\beta1$, $Ca_v\beta2$, $Ca_v\beta3$, and $Ca_v\beta4$) show distinct tissue and subcellular distributions (Dolphin, 2003; Buraei and Yang, 2010). $Ca_v\beta$ subunits interact with the 18-aa $\alpha1$ interaction domain (AID) of the cytoplasmic linker between internal repeats I and II of the pore-forming α_1 subunit (Pragnell et al., 1994; Chen et al., 2004; Opatowsky et al., 2004; Van Petegem et al., 2004). $Ca_v\beta$ subunits enhance VGCC channel activity (Mori et al., 1991; Chien et al., 1995; Josephson and Varadi, 1996; Kamp et al., 1996; Brice et al., 1997; Jones et al., 1998; Colecraft et al., 2002), not only by facilitating cell surface transport of VGCCs and by preventing ER-associated protein degradation (Altier et al., 2011) but also by modulating their gating properties (Buraei and Yang, 2010).

VGCCs interact via the $Ca_v\alpha1$ subunit with several pre- and postsynaptic proteins, including SNAP-25, synaptotagmin, syntaxin, Mint, and calcium/calmodulin-dependent serine protein kinase (Sheng et al., 1994; Bezprozvanny et al., 1995; Zhong et al., 1999; Maximov and Bezprozvanny, 2002; Spafford and Zamponi, 2003; Nishimune et al., 2004; Kang et al., 2006). The interaction and clustering of VGCCs with components of the secretory vesicle docking and fusion machinery by multiprotein adaptors highlights the importance of the spatial and temporal coordination of Ca^{2+} entry and neurosecretion (Yang and Berggren, 2006). The $Ca_v\beta$ subunits also interact with regulatory proteins that inhibit (e.g., RGK proteins, calcium, heterotrimeric G proteins, opioid receptor–like receptor 1, and several synaptic proteins) or facilitate VGCC activity (e.g., Rim1) or both (e.g., calmodulin; Herlitze et al., 1996; Ikeda, 1996; Lee et al., 1999; Béguin et al., 2001, 2005a,b, 2006, 2007; Beedle et al., 2004; Chen et al., 2005; Finlin et al., 2005; Evans and Zamponi, 2006; Jarvis and Zamponi, 2007; Kiyonaka et al., 2007; Buraei and Yang, 2010; Flynn and Zamponi, 2010; Yang et al., 2010).

Here, we describe a previously uncharacterized protein, which we term the VGCC–β-anchoring and -regulatory protein (BARP), and characterize its role in the regulation of VGCC activity and Ca^{2+}-regulated exocytosis. BARP is highly expressed in several specific neuronal populations and neuropeptide secretory cells, plays a role in the recruitment of $Ca_v\beta$ subunits to the plasma membrane, and negatively regulates VGCCs by interfering with the association of the $Ca_v\beta$ subunit with the $Ca_v\alpha1$ subunit. We hypothesize that BARP serves as an adaptor protein that modulates $Ca_v\beta$ subunit localization and their association with $Ca_v\alpha1$ subunits to regulate VGCC activity.

Results

Identification, tissue-specific expression, and membrane topology of BARP

BARP was identified in a yeast two-hybrid screen of a mouse insulin-secreting MIN6 cell cDNA library using $Ca_v\beta3$ as bait. BARP is encoded by an open reading frame of unknown function, C19orf26, which, based on its chromosomal location, has also been referred to as Dos (downstream of Stk11 kinase; Gerhard et al., 2004). Sequence analysis of EST clones and cDNA cloned from libraries revealed a ~3-kb transcript, coding for a 698-aa protein. BARP contains no known functional domains except for a single putative transmembrane domain and a putative N-glycosylation site (Figs. 1 A and S1 A). High BARP mRNA levels were found in brain, pancreatic islets, and neuroendocrine cell lines (MIN6 and PC12), with undetectable or weak expression in other tissues (Fig. 1 B).

The presence of BARP protein was confirmed in brain and PC12 cells using a polyclonal (72) and two affinity-purified mAbs (12B1 and 8B2) raised against different regions of the protein (Fig. 1 C). Specificity of the different antibody (Ab) was validated by the lack of staining in untransfected cells (Fig. S1 B) or after preabsorbing the Ab on a GST-BARP fusion protein (Figs. S1 C and S2 B) and by the absence of reactivity in pancreas-specific BARP knockout mice (Fig. S2 C). In COS-1 cells transfected with a Myc-tagged BARP cDNA, the labeling of the three Abs predominantly colocalized with that of the anti-Myc Ab (Fig. S1 B), but the BARP Ab did not colocalize with a Myc-tagged β-galactoside used as a negative control.

The predicted initiation methionine for BARP (M1; Fig. S1 A) is in accordance with the high quality annotation of the protein coding regions of the mouse and human genome by the Consensus Coding Sequence Project (Pruitt et al., 2009). This is the first conserved Met and the site where the high degree of amino acid identity among BARPs from different species starts (Fig. S1 D). In agreement with M1 being the initiation methionine, expression in COS-1 cells of mutants lacking either M7 or M80, the only two other conserved putative translation initiation sites in BARP, showed the same electrophoretic mobility as wild-type (WT) BARP, consistent with initiation of translation from M1 (Fig. S1 D). In contrast, the mobility of the M1A mutant was detectably faster than WT BARP, presumably because in the absence of M1, initiation can occur from M7. A truncated translation product was also obtained from the M1A/M7A mutant, presumably as a result of translation from M80 because only mutation of all three conserved methionine residues abolished translation. Thus, although M1, M7, and M80 can act as independent initiation sites, in the full-length cDNA, the codon for M1 serves as the main site for the initiation of translation.

BARP overexpressed in COS-1 or human embryonic kidney–derived tsA201 cells migrated as a doublet of higher molecular mass as compared with the in vitro translated BARP (Fig. 1 D), suggestive of posttranslational modifications. In PC12 cells, the upper band was more prominent. Tunicamycin led to a reduction of the apparent molecular mass for WT BARP but not for a mutant lacking the putative N-glycosylation site (^{25}N-X-S/T), consistent with the presence of N-linked glycosylation (Fig. 1 E). For better resolution of the different bands by SDS-PAGE, a C-terminal truncation of BARP (C-tr145, consisting of aa 1–145) was analyzed. After tunicamycin, PNGase F, or Endoglycosidase H treatment, the truncated form of BARP co-migrated with the truncated form lacking the N-glycosylation site (Fig. S1 E), confirming the presence of this glycosylation. After these treatments, however, BARP still migrated as a doublet, indicating the existence of additional unknown posttranslational modifications or internal initiation of translation.

The presence of N-terminal carbohydrate chains suggested that BARP is a type I membrane protein, with the N terminus located on the extracellular side. This topology was validated by cell surface labeling experiments, in which N- or C-terminally Myc-tagged BARP was expressed in COS-1 cells and the cells

Published April 21, 2014

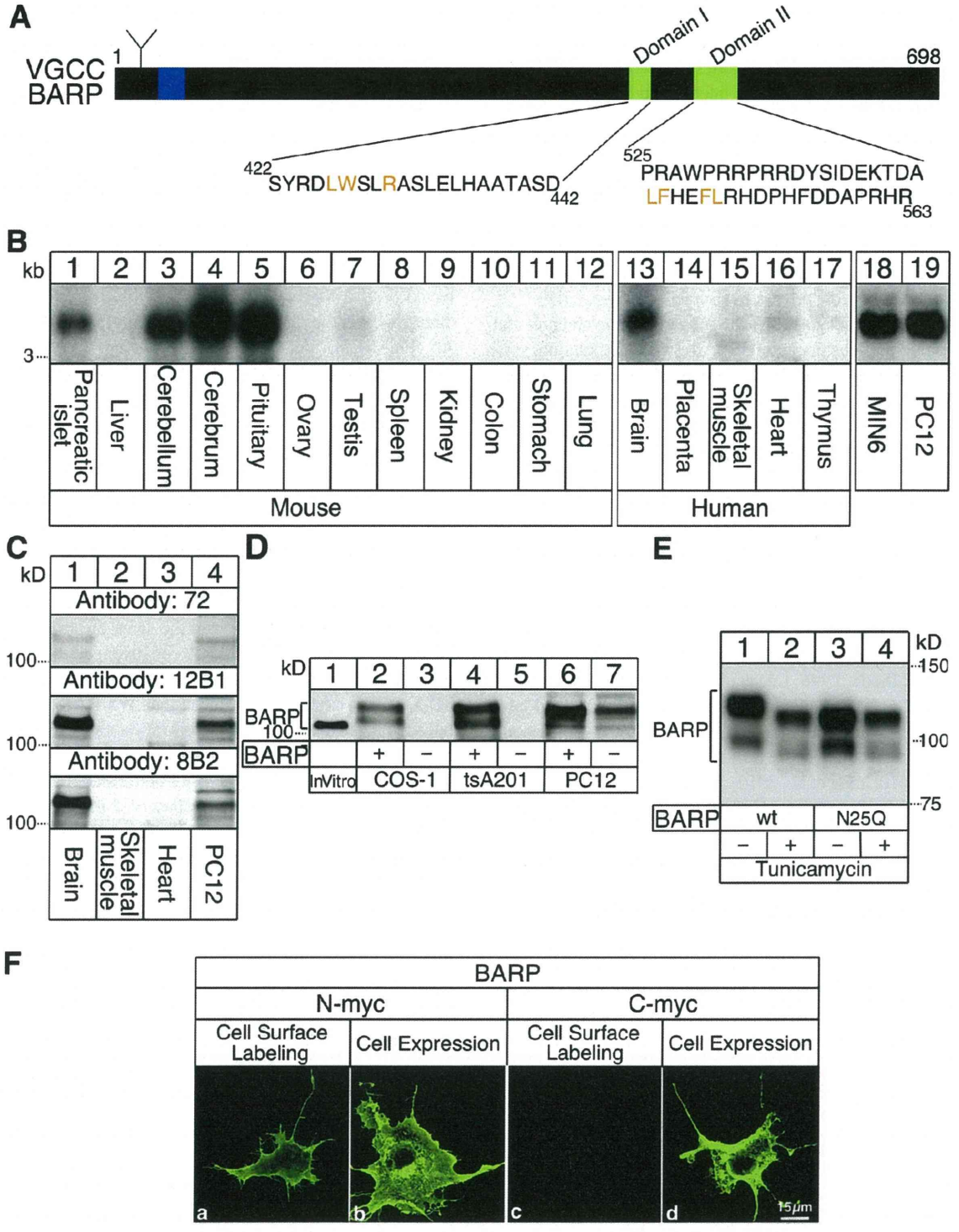

Figure 1. **Characterization of BARP.** (A) Structural and functional domains. The N-glycosylation site (Y), transmembrane region (blue), and the $Ca_v\beta$-interacting domain I and II (green) are depicted. Amino acid sequences of domain I and II, with residues crucial for interaction with $Ca_v\beta$ are in orange. (B) Northern blot analysis. BARP mRNA expression was analyzed in the indicated mouse and human tissues and cell lines. The samples were run on three separate gels, as shown. (C) WB analysis. Endogenous BARP protein was detected in brain and PC12 cells by WB using a rabbit polyclonal Ab (72) or two mouse mAb (12B1 and 8B2) raised against different regions of the protein. (D) Comparison of in vitro synthesized and cell-expressed BARP protein. BARP obtained by in vitro translation or from transfected COS-1, tsA201, or PC12 cells was analyzed by SDS-PAGE and WB (mAb 12B1). (E) BARP is N-glycosylated on Asn25. COS-1 cells expressing WT BARP or a BARP mutant lacking the putative N-glycosylation site (N25Q) were treated with tunicamycin to inhibit N-glycosylation. Cell lysates were analyzed by Tris/acetate-PAGE WB (Ab 72). (F) Membrane topology of BARP. Nonpermeabilized (cell surface labeling) or permeabilized (cell expression) are depicted. COS-1 cells expressing N- or C-Myc BARP were stained with an Ab to Myc and visualized by immunofluorescence microscopy. In nonpermeabilized cells (a and c), only the N-terminally tagged BARP was detected.

Published April 21, 2014

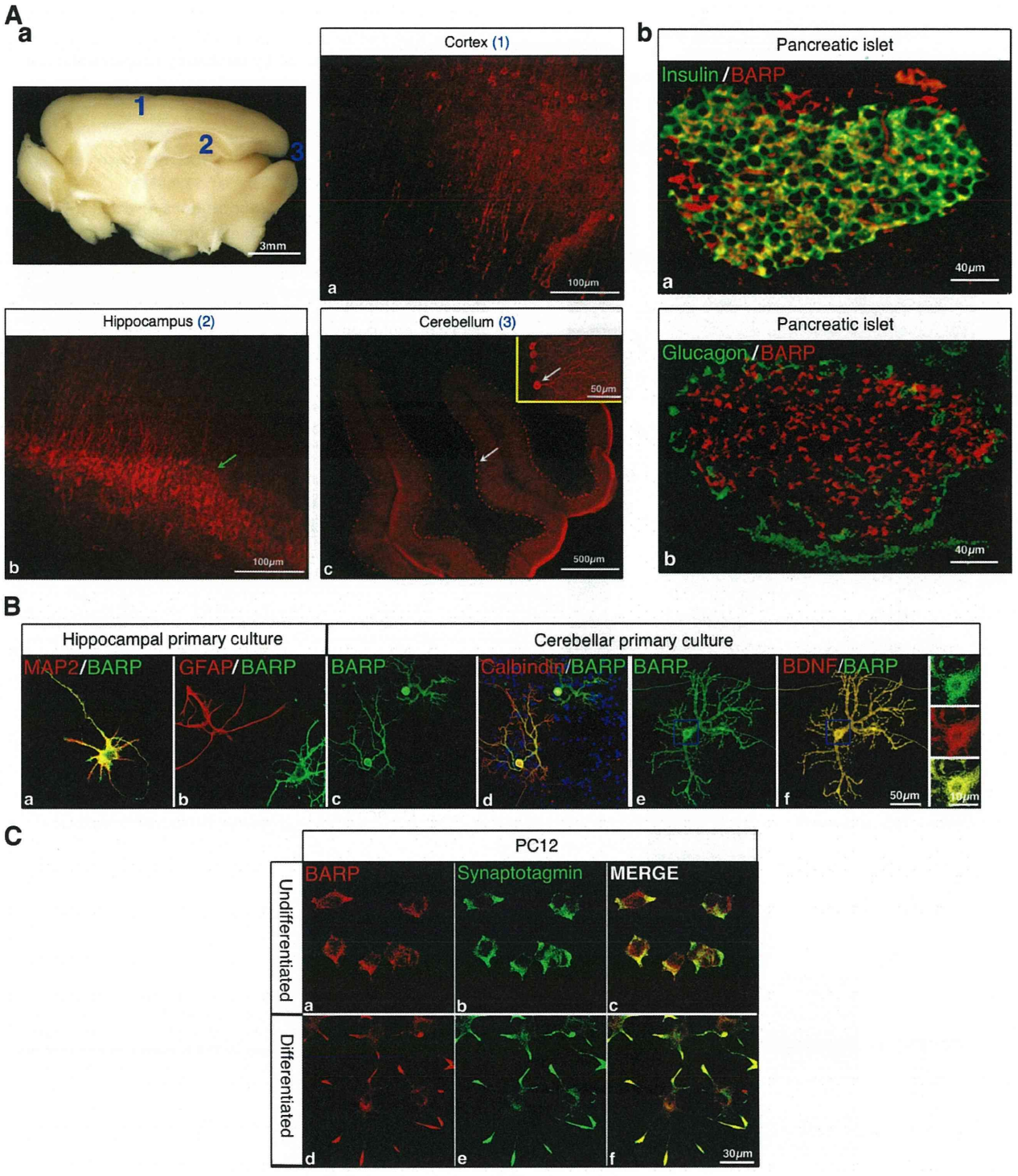

Figure 2. **Neuronal expression of BARP.** (A) Expression of BARP in brain (a) and pancreatic islets (b). Sections of cortex (1), hippocampus (2), and cerebellum (3) stained for BARP (mAb 12B1) and analyzed by immunofluorescence microscopy. BARP is detected in cell bodies and the dendritic extensions of Purkinje (white arrows) and pyramidal (green arrow) cells. In pancreatic islets, BARP is expressed in insulin-positive β cells but absent from α cells labeled for glucagon. The inset shows a higher magnification of the Purkinje cell layer. (B) Neuronal expression of BARP. Primary cells isolated from hippocampus or cerebellum were costained with mAb 12B1 to BARP and Ab to the neuronal marker MAP2 (a), the glial marker GFAP (b), the Purkinje marker calbindin (d), or the dense core vesicle protein BDNF (f). The insets show a higher magnification of the vesicular staining in the soma. Nuclei were stained with Hoechst (blue). (C) Colocalization of BARP with synaptotagmin in PC12 cells. Control or NGF-differentiated PC12 cells were costained with Ab to the regulated secretory vesicle marker synaptotagmin and BARP (Ab 72) and analyzed by confocal microscopy.

Published April 21, 2014

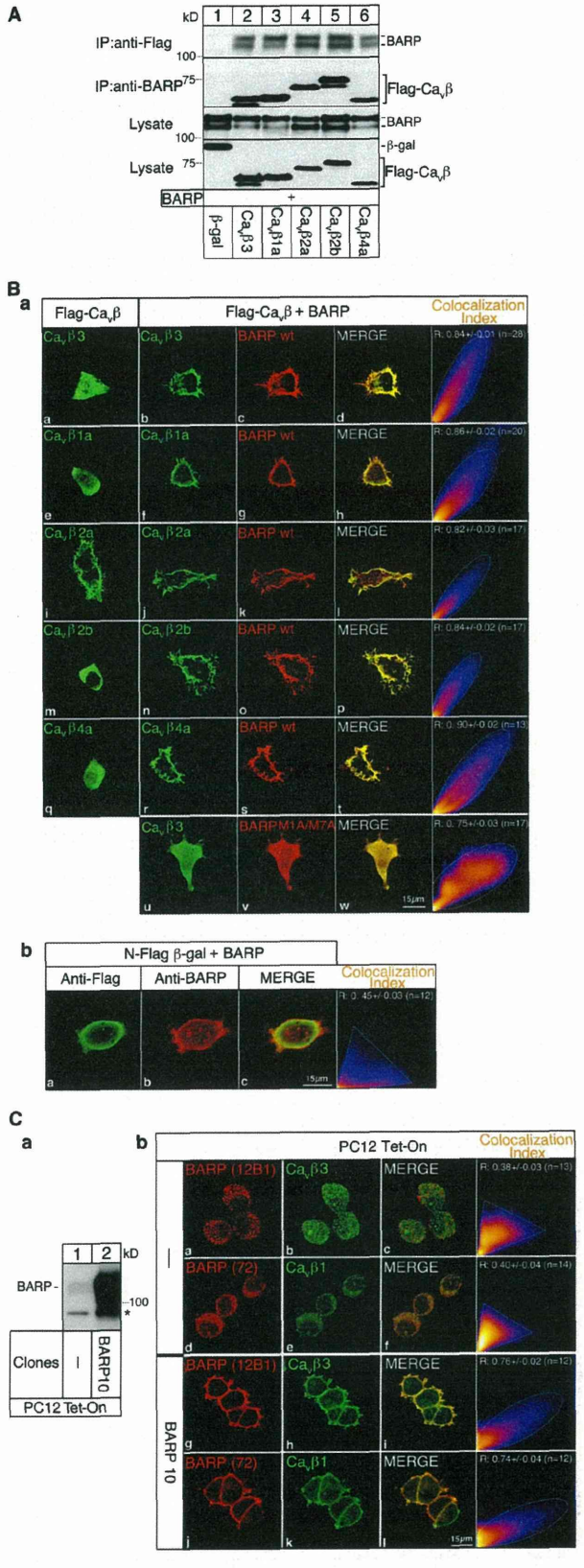

Figure 3. **BARP binds and localizes Ca$_v$β subunits to the plasma membrane.** (A) Coimmunoprecipitation of Ca$_v$β and BARP. COS-1 cells were cotransfected with cDNAs for BARP and the different Flag-tagged Ca$_v$β subunit or, as a control, Flag–β-galactosidase (β-gal). Flag-tagged proteins were immunoprecipitated (IP), and bound BARP was detected by WB (Ab 72). The association was confirmed by reciprocal immunoprecipitation. Aliquots of cell lysates were analyzed by WB to monitor protein expression. (B) BARP localizes Ca$_v$β subunits to the plasma membrane. (a) PC12 cells were transfected with cDNAs for the different Flag-Ca$_v$β subunits, either alone or with a Myc-BARP cDNA. Cells were analyzed by immunofluorescence microscopy using Ab to Flag and Myc to detect the Ca$_v$β subunits and BARP, respectively. Colocalization index is shown in the rightmost images. (b) Costaining of PC12 cells cotransfected with cDNAs for N-Flag–β-galactosidase, and Myc-BARP cDNA served as a negative control. (C) Constitutive overexpression of BARP relocates endogenous Ca$_v$β subunits. (a) Protein expression. WB analysis of lysates from control PC12 Tet-On cells or cells constitutively expressing BARP. The asterisk indicates a nonspecific protein band. (b) Localization of endogenous Ca$_v$β subunits to the plasma membrane upon BARP expression. Endogenous Ca$_v$β subunits and endogenous (a–f) or stably overexpressed BARP (g–l) in PC12 Tet-On cell lines were detected by immunofluorescence microscopy. Colocalization index is shown in the rightmost images. The dotted lines delimit the cloud shape of the colocalization index. Note that imaging of endogenous BARP required a 10× longer exposure to obtain a comparable intensity to overexpressed BARP.

were labeled with antitag Ab either before (cell surface labeling) or after (cell expression) cell permeabilization. Only N-terminally tagged BARP was detected by incubating nonpermeabilized intact cells with Ab to Myc, thus confirming the extracellular exposure of the N terminus (Fig. 1 F).

Neuronal and pancreatic expression and subcellular localization of BARP

Immunolabeling of mouse tissue sections revealed BARP protein in the cortex, cerebellum, and hippocampus of the brain (Fig. 2 A, a) and in pancreatic islets (Figs. 2 A, b; and S2 C), consistent with the Northern blot analysis (Fig. 1 B). During mouse development, BARP expression in the brain peaked between embryonic day 18 (E18) and postnatal day 7 (P7; Fig. S2 A). In the cortex and hippocampus, BARP was detected in pyramidal cell bodies and dendrites. In the cerebellum, BARP was exclusively expressed in Purkinje cells, uniformly in soma and the main dendritic shaft and as a patchy staining along the distal dendrites (Figs. 2 A, a; and S2 B). Costaining of cultured primary cells isolated from hippocampus and cerebellum with BARP and neuronal (MAP2 and calbindin) or glial (glial fibrillary acidic protein [GFAP]) markers confirmed the neuron-specific expression of BARP (Fig. 2 B). In cerebellar primary cells, BARP was present in calbindin-positive Purkinje cells, where it localized to the cell soma, the dendritic shaft, and along the axon, including the presynaptic button, and colocalized with the dense core vesicle marker brain-derived neurotrophic factor (BDNF).

In PC12 cells, BARP partially colocalized with the Ca^{2+}-dependent secretory vesicle markers synaptotagmin I and, upon NGF-induced differentiation, localized to the growth cone (Fig. 2 C). In contrast to the more prominent vesicular staining of endogenous BARP in PC12 cells (Fig. 3 C, b), BARP overexpressed in PC12 or other cell lines was enriched at the plasma membrane (Fig. S2, D and F). Such a difference in distribution was also reported for endogenous versus overexpressed synaptotagmin I (Vega and Hsu, 2001) and could be reproduced in our PC12 cells (compare Figs. 2 C and S2 D). This was interpreted

Published April 21, 2014

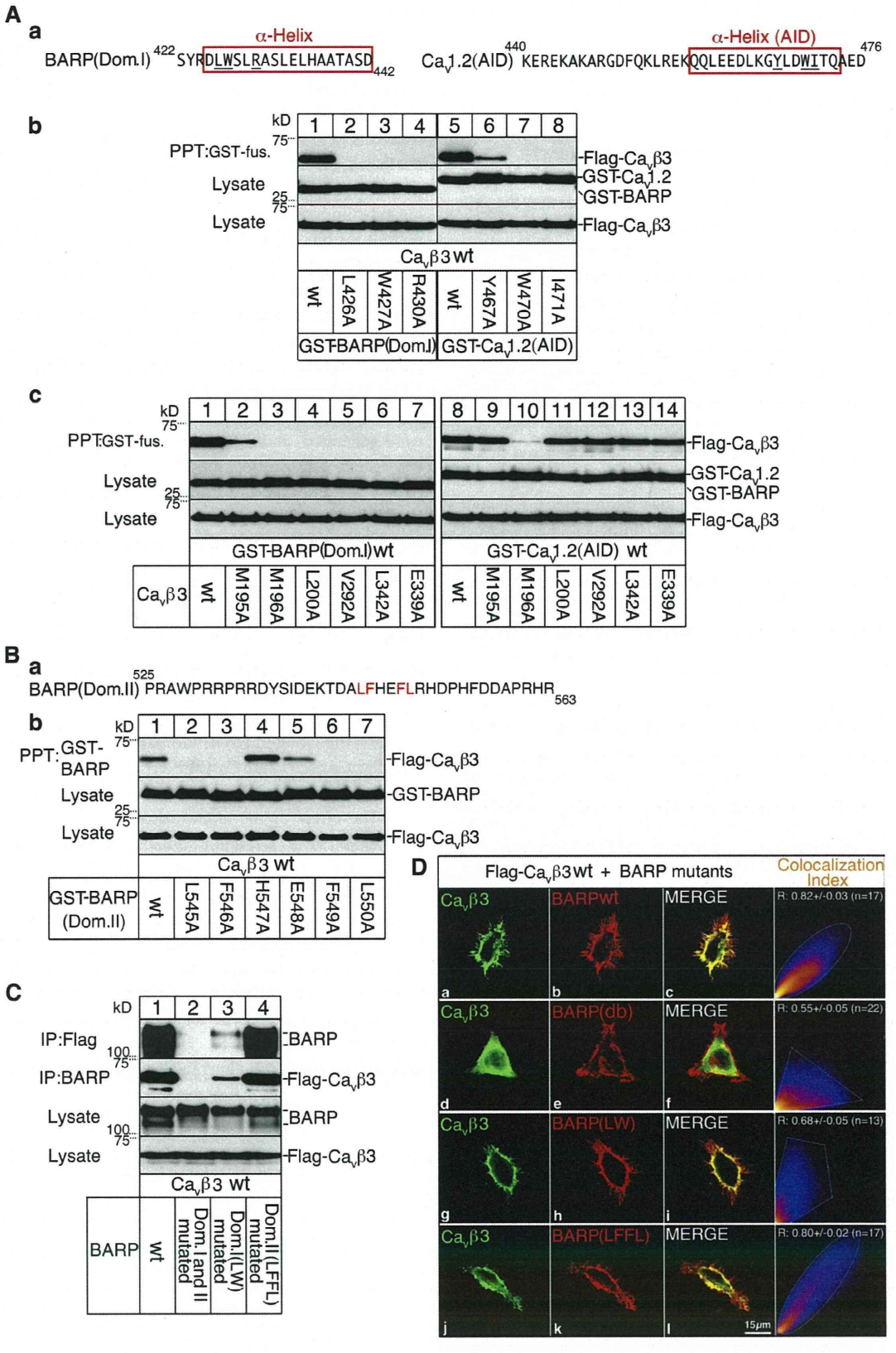

Figure 4. **BARP associates with $Ca_v\beta$ subunits via domain I and domain II.** (A) Identification of BARP domain I (Dom.I) as a $Ca_v\beta$-interacting domain. (a) Amino acid sequence of domain I and AID. The predicated (BARP) or known ($Ca_v1.2$ AID) α helix and amino acids important for $Ca_v\beta$ binding (underlined) are shown. (b) Identification of amino acids in domain I important for binding to the $Ca_v\beta$. COS-1 cells expressing Flag-$Ca_v\beta3$ and WT or mutated

Published April 21, 2014

to reflect a shift in the steady-state distribution from a more prominent vesicular to a more pronounced plasma membrane localization after overexpression (Han et al., 2004; Atiya-Nasagi et al., 2005).

BARP binds and localizes the different $Ca_v\beta$ subunit isoforms to the plasma membrane

Coimmunoprecipitation experiments using BARP and the different $Ca_v\beta$ subunit isoforms overexpressed in COS-1 cells established that BARP binds to all the different $Ca_v\beta$ isoforms (Fig. 3 A). These associations were corroborated in intact cells using immunofluorescence experiments. When overexpressed in PC12 (Fig. 3 B) or COS-1 (Fig. S2 E) cells, the $Ca_v\beta$ subunits showed, with the exception of $Ca_v\beta$2a, a cytosolic distribution with some degree of nuclear labeling for $Ca_v\beta$3 and $Ca_v\beta$4a (Dolphin, 2003). Remarkably, overexpression of BARP localized the cytosolic $Ca_v\beta$ isoforms to the plasma membrane. This confirms that the two proteins interact in a cellular context and shows that BARP can influence the subcellular distribution of $Ca_v\beta$ subunits in the absence of $Ca_v\alpha$1. The colocalization index, which in this context reflects the efficiency of recruitment of the different $Ca_v\beta$ subunits by BARP, did not drastically differ, indicating a similar effect of BARP for all isoforms. As a control, BARP M1A/M7A, which utilizes M80 for initiation of translation (Fig. S1 D) and thus lacks the first 79 aa and hence the transmembrane domain, failed to localize $Ca_v\beta$3 to the plasma membrane (Figs. 3 B, a; and S2 E).

When BARP was constitutively and stably overexpressed from a cytomegalovirus promoter in PC12 Tet-On cells (BARP10; Fig. 3 C, a), the localization of endogenous BARP changed from a vesicular pattern in parental cells to a prominent peripheral staining in BARP-overexpressing cells (Fig. 3 C, b). Concomitantly, endogenous $Ca_v\beta$1 and $Ca_v\beta$3, which poorly colocalized with endogenous BARP in untransfected cells, redistributed to the cell periphery upon BARP overexpression (Fig. 3 C, b).

BARP encodes two distinct $Ca_v\beta$-binding domains

To obtain additional insight into the mechanism by which BARP associates with VGCCs, the domains in BARP required for its interaction with the $Ca_v\beta$ subunit were identified. Deletion and alanine-scan mutagenesis of BARP combined with yeast two-hybrid screening (Fig. S3, A and B) and GST pull-down experiments (Fig. S3, C and E) narrowed down the interaction with $Ca_v\beta$ subunits to two domains, termed domain I and domain II. Based on in silico molecular dynamics simulations, domain I (aa 422–442; Fig. 4 A, a) is predicted to fold into an α helix (Fig. S3 D). Mutation of L426, W427, or R430 in BARP abolished the interaction of domain I with the $Ca_v\beta$ subunit (Fig. 4 A, b). The AID of the $Ca_v\alpha$1 subunit and mutants carrying substitutions of aa Y467, W470, and I471, known to be important for binding to $Ca_v\beta$ (Richards et al., 2004), served as a control (Fig. 4 A, a and b).

Previous studies, including crystallographic analysis, established that the AID is associated as an α helix with a hydrophobic groove in $Ca_v\beta$, also termed the AID-binding pocket (ABP; Pragnell et al., 1994; Chen et al., 2004; Richards et al., 2004; Van Petegem et al., 2004). To explore whether domain I could also bind to the ABP, mutations in this region of $Ca_v\beta$ were generated, and their effect on the interaction with BARP was tested. Substitutions of several amino acids in the hydrophobic pocket of the $Ca_v\beta$ subunit impaired its association with BARP domain I (Fig. 4 A, c). This was not caused by an effect of the mutations on the folding of $Ca_v\beta$ because, with the exception of M196A, the different $Ca_v\beta$ mutants still bound the AID.

Because a truncated BARP that lacked domain I still interacted with $Ca_v\beta$, analysis of additional BARP mutants (Fig. S3 E) led to the identification of a second binding region, domain II (aa 525–563; Fig. 4 B, a). Amino acid substitutions in domain II revealed two leucine-phenylalanine pairs (L545-F546 and F549-L550) as important for efficient $Ca_v\beta$ binding (Fig. 4 B). Interestingly, the isolated BARP domain II interacted with $Ca_v\beta$3, $Ca_v\beta$2a, $Ca_v\beta$2b, and $Ca_v\beta$4a but not with $Ca_v\beta$1a, whereas domain I bound all $Ca_v\beta$ subunits tested (Fig. S3 F).

The effect of the amino acids substitutions in domain I (L426A and W427A) and/or domain II (L545A, F546A, F549A, and L550A) on the association with $Ca_v\beta$ was next analyzed in full-length BARP. Simultaneous mutation of both domains abolished the association of the mutated BARP with the $Ca_v\beta$ (Fig. 4 C). Although the interaction between BARP and $Ca_v\beta$ was more sensitive to the disruption of domain I, the presence of one intact domain was sufficient to confer not only detectable binding but also plasma membrane localization of the $Ca_v\beta$ subunits in cells (Figs. 4 D and S3 H). However, the colocalization index suggests that domain II alone mediates a less efficient localization

GST-BARP domain I were lysed, GST fusion (fus.) proteins were precipitated, and the associated $Ca_v\beta$3 was detected by WB. As a control, $Ca_v\beta$3 was coprecipitated with WT or mutated GST-Ca_v1.2 AID. Aliquots of cell lysates were analyzed by WB to monitor protein expression. The black line indicates the rearrangement of lanes for presentation purposes. (c) Identification of amino acids in $Ca_v\beta$3 important for binding to BARP domain I. COS-1 cells expressing GST-BARP domain I or GST-AID with mutated Flag-$Ca_v\beta$3 were lysed, GST fusion proteins were precipitated, and associated $Ca_v\beta$3 was detected by WB. Aliquots of cell lysates were analyzed by WB to monitor protein expression, using two separate gels, as shown. PPT, precipitation. (B) Identification of BARP domain II as a second $Ca_v\beta$ subunit binding region. (a) Amino acid sequence of domain II with residues crucial for the association with $Ca_v\beta$ (red). (b) Identification of amino acids in domain II important for $Ca_v\beta$ binding. COS-1 cells expressing Flag-$Ca_v\beta$3 and WT or mutated GST-BARP domain II were lysed, GST-BARP domain II was precipitated, and the associated Flag-$Ca_v\beta$3 was detected by WB. Aliquots of cell lysates were analyzed by WB to monitor protein expression. (C) Role of domains I and II in the context of full-length BARP in $Ca_v\beta$ binding. COS-1 cells expressing WT BARP or the BARP domain I and/or domain II mutants and Flag-$Ca_v\beta$3 were lysed, Flag-$Ca_v\beta$3 was immunoprecipitated (IP), and the associated BARP was revealed by WB (Ab 72). In a reciprocal experiment, BARP was immunoprecipitated, and bound Flag-$Ca_v\beta$3 was detected. Aliquots of cell lysates were analyzed by WB to monitor protein expression. (D) Roles of domains I and II in the context of full-length BARP in $Ca_v\beta$3 membrane recruitment. PC12 cells expressing Flag-$Ca_v\beta$3 and either BARP WT or mutants affecting domain I and/or domain II were labeled with Ab to Flag (green) and BARP (Ab 72) and processed for immunofluorescence microscopy. Colocalization index is shown in the rightmost images. The dotted lines delimit the cloud shape of the colocalization index. (d–f) Mutation of both domains I and II (db) in BARP abolishes the localization of $Ca_v\beta$3 to the plasma membrane.

Published April 21, 2014

of $Ca_v\beta3$ to the plasma membrane (0.68 ± 0.05) compared with WT BARP (0.80 ± 0.02) or BARP with domain II mutated (0.80 ± 0.02, $P < 0.05$).

BARP modulates the interaction between the $Ca_v\beta$ and $Ca_v\alpha1$ subunits

Because BARP domain I binds to the ABP in $Ca_v\beta$, BARP may interfere with the interaction between $Ca_v\beta$ and $Ca_v\alpha1$. To test this hypothesis, we monitored the stability of a preassembled complex between the $Ca_v\beta_3$ and a GST-AID fusion protein after addition of competitive peptides coding for domain I or, as a control, the AID. Indeed, $Ca_v\beta3$ was displaced by soluble domain I or AID peptides from the immobilized GST-AID and recovered in the supernatant (Fig. 5 A), consistent with BARP domain I and the AID binding in a mutually exclusive manner to the same or an overlapping site in $Ca_v\beta$. Slightly higher concentrations of domain I peptide than AID peptide were required for disruption of the complex.

The biochemical results were corroborated in a cellular context by coexpressing BARP, $Ca_v\beta3$, and $Ca_v\alpha1$ and monitoring their associations in coprecipitation experiments. In the presence of WT BARP, the $Ca_v\beta3$ and $Ca_v\alpha1$ subunits no longer associated (Fig. 5 B). In contrast, coprecipitation was not affected in the presence of BARP with both domain I and II mutated. Mutation of either domain individually partially interfered with the association between the $Ca_v\beta3$ and $Ca_v\alpha1$, showing the importance of domain I and II. Interestingly, mutation of domain I alone allowed the detection of a ternary complex containing BARP, $Ca_v\alpha1$, and $Ca_v\beta3$ (Fig. 5 B, lane 3). As a control, neither $Ca_v\beta3$ nor BARP associated with a mutated $Ca_v\alpha1$ subunit unable to bind $Ca_v\beta3$ (Fig. S4 A), suggesting that BARP does not bind to $Ca_v\alpha1$ directly. Similar results were also obtained for $Ca_v\beta3$ in combination with other $\alpha1$ subunit subtypes (e.g., $Ca_v2.1$ and $Ca_v2.2$; Fig. S4, B and C) and for other $Ca_v\beta$ subunit isoforms (e.g., $Ca_v\beta1a$, $Ca_v\beta2a$, $Ca_v\beta2b$, and $Ca_v\beta4a$; Fig. S4 D).

Coimmunoprecipitation experiments from PC12 cells and the brain confirmed that also endogenous BARP and $Ca_v\beta3$ associate with each other (Fig. 5 C). Interestingly, comparison of the amount of endogenous $Ca_v\beta3$ that was bound to either endogenous or overexpressed BARP in PC12 cells suggested the presence of a significant pool of $Ca_v\beta3$ that is not associated with endogenous BARP. In addition to $Ca_v\beta3$, BARP associated with $Ca_v\beta4$ in cerebellum and cerebrum and to a lesser extent with $Ca_v\beta1$ in the latter (Figs. 5 D and S4 E).

BARP inhibits VGCC activity without affecting cell surface expression of VGCCs

$Ca_v\beta$ subunits modulate Ca^{2+} channel activity by increasing channel current density at the plasma membrane and/or facilitating the trafficking of newly synthesized $Ca_v\alpha1$ subunits from the ER to the plasma membrane (Chien et al., 1995; Dolphin, 2003). To explore the functional role of BARP in regulating VGCC activity, BHK cells stably expressing $Ca_v\alpha1$ ($Ca_v2.1$ or $Ca_v2.2$), $Ca_v\beta1a$, and $Ca_v\alpha2\delta$ subunits to reconstitute P/Q- or N-type VGCCs (Niidome et al., 1994) were transfected with or without WT or mutated BARP cDNAs (Fig. 6, A and B) and subjected to electrophysiological analysis. Compared with controls, in cells overexpressing WT BARP, but not BARP with domains I and II mutated, a drastic reduction in P/Q- or N-type channel Ca^{2+} currents was recorded (Figs. 6, A and B, a and c; and S5 A). Mutation of domain I or II individually resulted in a partial reduction of Ca^{2+} channel activity (Figs. 6, A and B, b and c; and S5 A). Inactivation kinetics in the presence or absence of WT BARP did not significantly differ (P/Q-type channel: control = 78 ± 12 ms, $n = 20$ [Kameyama et al., 1999]; WT BARP = 80 ± 23 ms, $n = 17$).

To analyze whether a defect in Ca^{2+} channel surface expression in the presence of BARP accounts for its inhibitory effect on Ca^{2+} currents, we monitored $Ca_v1.2$ trafficking in tsA201 cells. Similar to BHK cells expressing N or P/Q Ca^{2+} channel subtypes (Fig. 6, A and B), BARP inhibited Ca^{2+} channel activity in tsA201 cells coexpressing $Ca_v1.2$ and $Ca_v\beta3$ (Fig. 6 C). This inhibition was abrogated if both domains I and II were mutated and partially reduced if domain I or II was mutated independently.

Detection of $Ca_v1.2$ on the surface of nonpermeabilized intact tsA201 cells (Altier et al., 2002; Béguin et al., 2006) required coexpression with one of the $Ca_v\beta$ subunits (Figs. 6 D, a; and S5 B), and accordingly, mutation of the AID abolished Ca^{2+} channel cell surface transport (Fig. 6 D, a). Coexpression of $Ca_v1.2$ subunits with BARP, either in the absence or presence of $Ca_v\beta3$, did not significantly affect Ca^{2+} channel surface expression (Fig. 6 D, a). Relative cell surface expression of $Ca_v1.2$ in the presence or absence of $Ca_v\beta3$ and/or BARP was corroborated and quantified by coexpressing in tsA201 cells a $Ca_v\alpha1$ subunit carrying both a luminal (HA) and a cytosolic (EGFP) tag and measuring relative pixel intensities in intact and permeabilized cells (Fig. 6 D, b and c). Although $Ca_v\beta3$, either in the absence of presence of BARP, significantly increased the fraction of $Ca_v\alpha1$ at the cell surface (0.12 ± 0.02 vs. 0.39 ± 0.03, $P < 0.01$), BARP had no significant influence on $Ca_v1.2$ distribution (Fig. 6 C, c). Thus, BARP does not significantly interfere with the role of $Ca_v\beta$ in facilitating cell surface expression of Ca^{2+} channels and thus most likely inhibits channel activity at the plasma membrane.

BARP negatively modulates VGCC activity and Ca^{2+}-regulated secretion

To elucidate the role of BARP in physiological processes linked to VGCC function, we explored the effects of BARP on VGCC activity and Ca^{2+}-dependent hormone secretion in PC12 cells (Béguin et al., 2001). First, we took advantage of the observation that endogenous BARP expression varies in different PC12 clones and is higher in ATCC PC12 cells (CRL-1721) than in PC12 Tet-On cells (Takara Bio Inc.; Fig. 7 A, a). Correlating with the different BARP expression levels in these cells, endogenous Ca^{2+} channel current densities were lower in ATCC PC12 cells and significantly inhibited in PC12 Tet-On cells stably expressing BARP (Fig. 7 A, b). These results were corroborated in PC12 cells transiently expressing BARP. An almost complete reduction of endogenous Ca^{2+} currents was recorded in cells overexpressing WT BARP, whereas BARP with both domains I and II mutated had no significant effect on VGCC activity (Fig. 7 B).

Importantly, inhibition of VGCC activity by BARP had an effect on Ca^{2+}-triggered exocytosis (Fig. 7 C). Correlating with

Published April 21, 2014

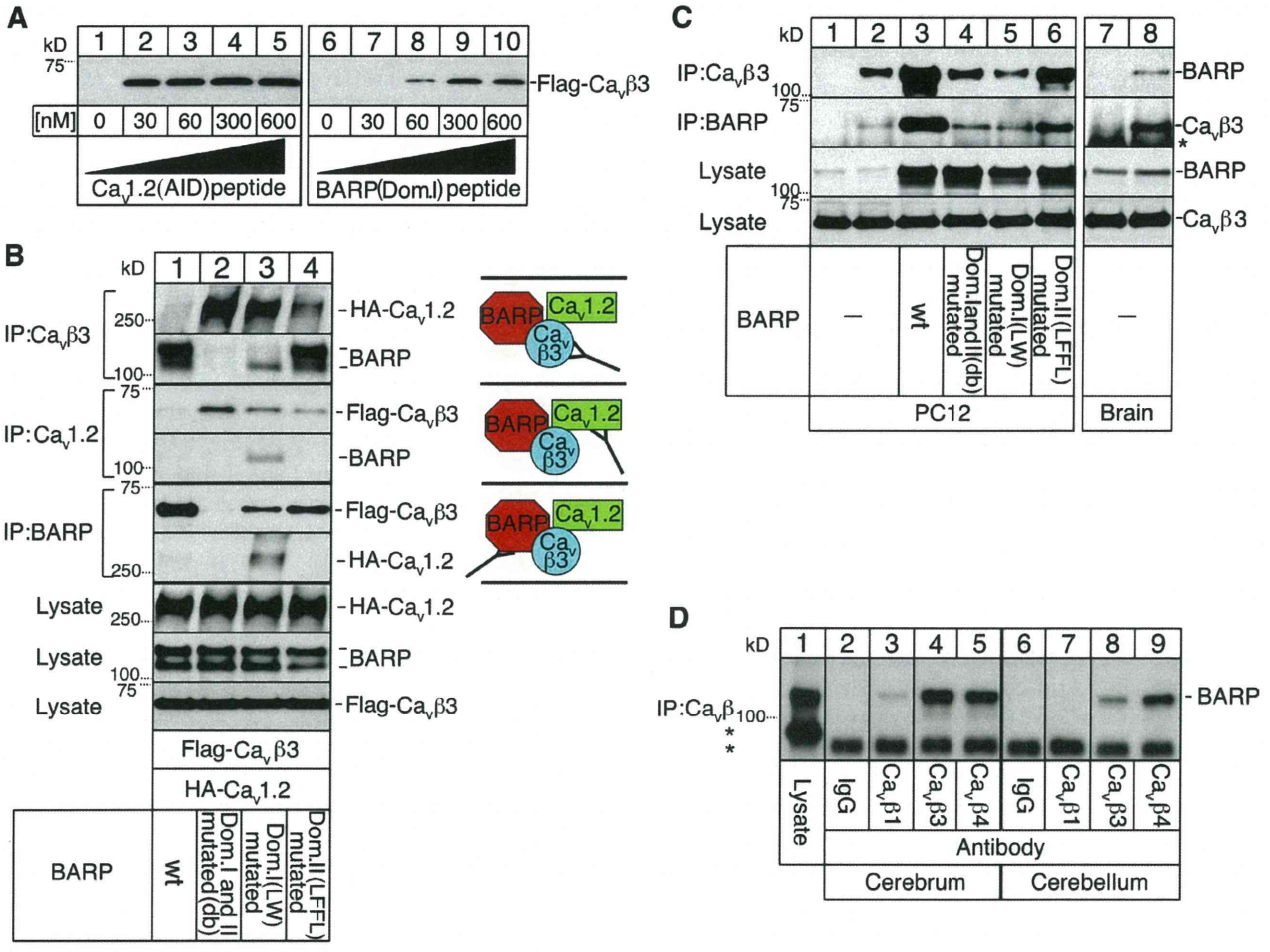

Figure 5. **Competition between the AID of $Ca_v\alpha1$ and BARP domain I for $Ca_v\beta$ binding and association of endogenous BARP and $Ca_v\beta$.** (A) BARP domain I (Dom.I) peptides dissociate a preformed AID–$Ca_v\beta3$ complex. Flag-$Ca_v\beta3$ expressed in COS-1 cells was isolated using a GST-AID fusion protein. The complex was incubated with increasing amounts of AID or BARP domain I peptide as indicated. Flag-$Ca_v\beta3$ displaced from the immobilized GST-AID was recovered in the supernatant and detected by WB using two separate gels, as shown. No Flag-$Ca_v\beta3$ was detected in the supernatant in the absence of peptides, showing that the immobilized $Ca_v\beta3$–AID complex did not dissociate over the duration of the experiment. (B) BARP overexpression interferes with the association between $Ca_v\beta$ and $Ca_v1.2$ subunits. COS-1 cells were cotransfected with cDNAs for WT or mutated BARP together with Flag-$Ca_v\beta3$ and HA-$Ca_v1.2$ subunits. Flag-$Ca_v\beta3$, HA-$Ca_v1.2$, or BARP was immunoprecipitated (IP), and the associated Ca^{2+} channel subunits or BARP was revealed by WB. Aliquots of cell lysates were analyzed by WB to monitor protein expression. db, both domains I and II mutated. (C) Association of endogenous BARP with $Ca_v\beta3$ in PC12 cells and brain. Endogenous $Ca_v\beta3$ was immunoprecipitated from PC12 cells or brain lysates, and the associated endogenous BARP was revealed by WB (mAb 12B1). In a reciprocal experiment, BARP was first immunoprecipitated (mAb 8B2), and bound $Ca_v\beta3$ was detected. Control IgG did not pull down BARP or $Ca_v\beta3$ (lanes 1 and 7). Aliquots of the cell lysates were analyzed by WB using two separate gels, as shown, to monitor the expression of endogenous or overexpressed proteins. The asterisk shows the band for IgG heavy chain. (D) Association of endogenous BARP with $Ca_v\beta1$, $Ca_v\beta3$, and $Ca_v\beta4$ in the cerebrum and cerebellum. Endogenous $Ca_v\beta$ subunits were immunoprecipitated from lysates, and the associated endogenous BARP was revealed by WB (mAb 12B1). Control IgG did not pull down BARP (lanes 2 and 6). Aliquots of the cell lysates were analyzed by WB to monitor BARP expression. Black lines indicate the rearrangement of lanes for presentation purposes. In addition, note that lane 1 represents a shorter exposure of the same membrane than the other lanes. The asterisks show the band for IgG heavy chain and a nonspecific band that did not coprecipitate with $Ca_v\beta$.

the Ca^{2+} channel recordings, overexpression of BARP strongly inhibited Ca^{2+}-dependent growth hormone secretion. Mutation of either domain I or II individually led to intermediate effects, whereas BARP carrying mutations in both $Ca_v\beta$ subunit binding sites only marginally affected growth hormone secretion.

Relative cell surface expression of $Ca_v1.2$ in the presence or absence of $Ca_v\beta3$ and/or BARP was also analyzed in PC12 cells as described for tsA201 cells (Fig. 6 D, b and c). Although $Ca_v\beta3$, either in the absence or presence of BARP, significantly increased the fraction of $Ca_v\alpha1$ at the cell surface (0.22 ± 0.01 vs. 0.45 ± 0.01, $P < 0.01$), BARP had no significant influence on $Ca_v1.2$ channel distribution in PC12 cells (Fig. 7 D). Collectively, these data establish BARP as a negative regulator of Ca^{2+}-dependent exocytosis, most likely by modulating VGCC activity at the plasma membrane.

Silencing of BARP enhances VGCC activity and Ca^{2+}-evoked secretion

We next analyzed the effect of silencing BARP in ATCC PC12 cells because these express significant levels of the protein endogenously (Fig. 7 A, a). Three shRNAs (A, B, and C) that target different regions of the BARP mRNA (Fig. 8 A, a) were stably transfected into PC12 cells, and two independent clones for each shRNA were selected. Expression levels of BARP in

Published April 21, 2014

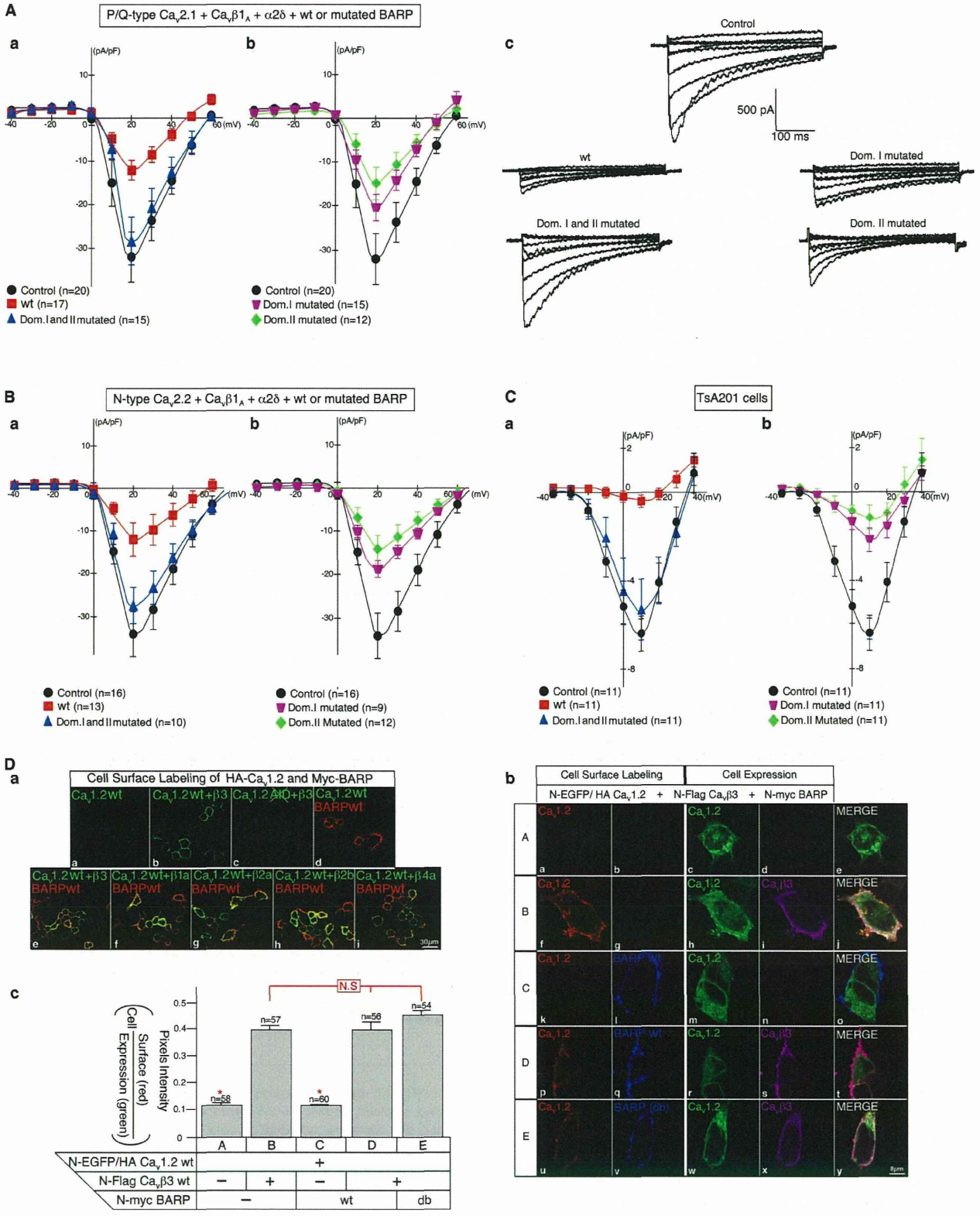

Figure 6. **BARP down-regulates voltage-gated Ca^{2+} channel activity without affecting its cell surface expression.** (A–C) BARP down-regulates VGCC activity. Effect of BARP on activity of P/Q (A)- or N (B)-type Ca^{2+} channels reconstituted in BHK cells or on VGCCs in tsA201 cells (C). (A and B) BHK cells stably expressing $Ca_v2.1$ (P/Q type) or $Ca_v2.2$ (N type) together with $Ca_v\beta1a$ and $Ca_v\alpha2\delta$ were transfected with a vector carrying WT or mutated BARP and EGFP cDNAs, and cells expressing EGFP were selected for electrophysiology. (C) tsA201 cells were cotransfected with a vector carrying WT or mutated BARP and mCherry cDNAs, a vector containing $Ca_v1.2$, and an internal ribosomal entry site followed by $Ca_v\beta3$ and EGFP cDNAs, and cells expressing mCherry and EGFP were selected for electrophysiology. Current–voltage (I–V) relationships of the different Ca^{2+} channels in the different cells

Published April 21, 2014

the six PC12 clones analyzed ranged between 10 and 25% of controls (Fig. 8 A, b and c), and VGCC Ca^{2+} current densities in these clones were between 50 and 140% higher than in controls (Fig. 8 A, d). The stimulatory effect of the shRNAs on VGCC activity could be suppressed by transfecting a rescue mouse BARP cDNA not targeted by the shRNAs (Fig. 8 A, d, red bars).

Endogenous BARP expression was also silenced by transient transfection of PC12 cells with a combination of two siRNAs (Fig. 8 B, a and b). Neurotransmitter release in these cells was analyzed to determine whether the Ca^{2+}-evoked secretion was also affected by silencing BARP. No significant differences in the basal secretion of acetylcholine were apparent between control and BARP siRNA–transfected cells (Fig. 8, c). However, upon stimulation with high K^+ to depolarize the plasma membrane and in turn activate VGCCs, an almost twofold higher secretion of the neurotransmitter was observed in BARP siRNA–transfected PC12 cells as compared with controls. These results are thus consistent with a negative regulatory role for BARP on VGCC activity and Ca^{2+}-regulated secretion.

Discussion

The biochemical and functional data presented establish BARP as a novel VGCC regulatory protein that exerts its effect by binding to $Ca_v\beta$ subunits and thereby interferes with the association of $Ca_v\beta$ with $Ca_v\alpha1$, leading to the inhibition of Ca^{2+} channel activity. Two domains in BARP associate with $Ca_v\beta$. Mutation of domain I to abolish its interaction with $Ca_v\beta$ allows BARP to associate, via domain II, with $Ca_v\beta$ and $Ca_v\alpha1$ to form a ternary complex. This ternary complex is not detected in the presence of a functional domain I, likely because domain I prevents a stable association between $Ca_v\alpha1$ and $Ca_v\beta$, and could thus in vivo be short lived or transient. Domain I is predicted to acquire an α-helical structure that interacts with the ABP in $Ca_v\beta$. In vitro, the binding between domain I and the ABP occurs in the nanomolar range and is of lower apparent affinity than the binding of the AID to $Ca_v\beta$, which ranges from 2 to 54 nM, depending on the particular $Ca_v\alpha1$ and $Ca_v\beta$ species (De Waard et al., 1995; Bell et al., 2001; Cantí et al., 2001; Geib et al., 2002; Opatowsky et al., 2003). In cells, however, evidence suggests that the $Ca_v\alpha1$ and $Ca_v\beta$ interaction has a lower affinity and is reversible (Hidalgo et al., 2006; Buraei and Yang, 2010). A local concentration of BARP (e.g., domain I) could thus be sufficiently high to modulate the $Ca_v\alpha1$ AID–$Ca_v\beta$ interaction. Alternatively, a cooperative binding of domains I and II could increase the affinity of BARP for the $Ca_v\beta$, and/or domain II binding could alter the conformation of $Ca_v\beta$ and thereby lower the affinity of $Ca_v\beta$ for the AID (Fig. S5 D). Consistent with this hypothesis, cellular overexpression of BARP abolished the association between $Ca_v\beta$ and $Ca_v\alpha1$ only if domain II–mediated binding was preserved. Posttranslational modifications of BARP or a binding protein may also regulate the cooperation between domains I and II for $Ca_v\beta$ association. The region in $Ca_v\beta$ that interacts with domain II has not been identified but could involve the SH_3 and/or HOOK domain because they show the highest divergence between $Ca_v\beta1a$, which does not bind domain II, and the other $Ca_v\beta$ isoforms (Fig. S3 G).

In the hippocampus and Purkinje cells, in which BARP is expressed, $Ca_v\beta1$ is mostly present in soma and dendrites, whereas $Ca_v\beta3$ and $Ca_v\beta4$ are found in axons and other parts of the neurons (Obermair et al., 2010). Interestingly, in the cerebrum and cerebellum, BARP coprecipitated with $Ca_v\beta3$ and $Ca_v\beta4$ but not, or only to a lesser extent, with $Ca_v\beta1$, suggesting that BARP may associate with specific $Ca_v\beta$ subunits in particular subcellular domains of neurons. For instance, BARP colocalized with BDNF, indicating its presence on dense core vesicles (Dieni et al., 2012). Intriguingly, during mouse development, BARP expression in the brain peaks between E18 and P7, a period crucial for neural circuit formation and synaptogenesis (Ullian et al., 2004; Christopherson et al., 2005).

$Ca_v\beta$ subunits facilitate surface expression of L-type VGCC by preventing ER-associated protein degradation of Cav1.2 (Altier et al., 2011). In tsA201 and PC12 cells, BARP inhibits VGCC activity without significantly altering the distribution of the $Ca_v\alpha1$ subunit between the cell surface and intracellular compartments and is thus unlikely affecting ER exit and stability of $Ca_v\alpha1$. However, it is well documented that $Ca_v\beta$ plays an important role in modulating, mainly via the IS6-AID linker, not only VGCC trafficking but also gating, including voltage-dependent activation, inactivation, and facilitation kinetics (Buraei and Yang, 2010). For instance, RGK GTPases, through association with $Ca_v\beta$ and/or $Ca_v\alpha1$, not only regulate cell surface expression of VGCCs but also directly modulate currents of the channel at the plasma membrane by lowering channel opening probabilities and/or immobilizing VGCC voltage sensors (Fan et al., 2010; Yang et al., 2010). The time course of the macroscopic current in

expressing the different BARP proteins (a and b) as well as the traces for P/Q (c)- and N (Fig. S5 A)-type channel recordings are shown. Three independent experiments were performed each, and the data were combined to obtain the indicated *n* values. Shown are the means ± SEM. Paired Student's *t* test at 20 mV. For P/Q-type channels, control versus BARP WT or domain II mutated ($P < 0.01$) and control versus BARP domain I mutated ($P < 0.05$) are shown. For VGCCs in tsA201 cells, control versus BARP WT and domains I or II mutated ($P < 0.01$) are shown. For better readability, the data are plotted in two individual graphs; hence, the curve for the controls in a and b is identical. (D) BARP does not affect cell surface expression of Ca^{2+} channels in tsA201 cells. (a) Cell surface expression of HA epitope–tagged $Ca_v1.2$ and N-Myc–BARP was monitored in the presence or absence of $Ca_v\beta3$ by immunofluorescence microscopy. tsA201 cells were cotransfected with cDNAs for WT HA-$Ca_v1.2$ or an AID mutant defective in $Ca_v\beta3$ binding, Myc-BARP, and $Ca_v\beta$ isoforms. $Ca_v1.2$ and BARP expressed at the cell surface in nonpermeabilized cells were detected using Ab to the extracellular HA epitope in $Ca_v1.2$ and Myc in BARP. (b) Cell surface expression of N-EGFP/HA-$Ca_v1.2$ and N-Myc–BARP was monitored in the presence or absence of $Ca_v\beta3$. tsA201 cells were cotransfected with cDNAs for N-EGFP/HA-$Ca_v1.2$ alone (A) either together with N-Flag–$Ca_v\beta3$ (B) or N-Myc–BARP (C) or with Flag-$Ca_v\beta3$ and WT BARP or BARP with domains I and II mutated (D and E). $Ca_v1.2$ and BARP expressed at the cell surface in nonpermeabilized cells were detected using Ab to the extracellular HA epitope in $Ca_v1.2$ and Myc in BARP. Cellular expressions of EGFP-$Ca_v1.2$ and $Ca_v\beta3$ are shown. Merged images are shown on the right. (c) Quantification of channel cell surface expression is stated as the relative surface expression of HA versus EGFP-$Ca_v1.2$ (red/green). Unpaired Student's *t* test: *, $P < 0.01$. db, both domains I and II mutated; Dom., domain.

Published April 21, 2014

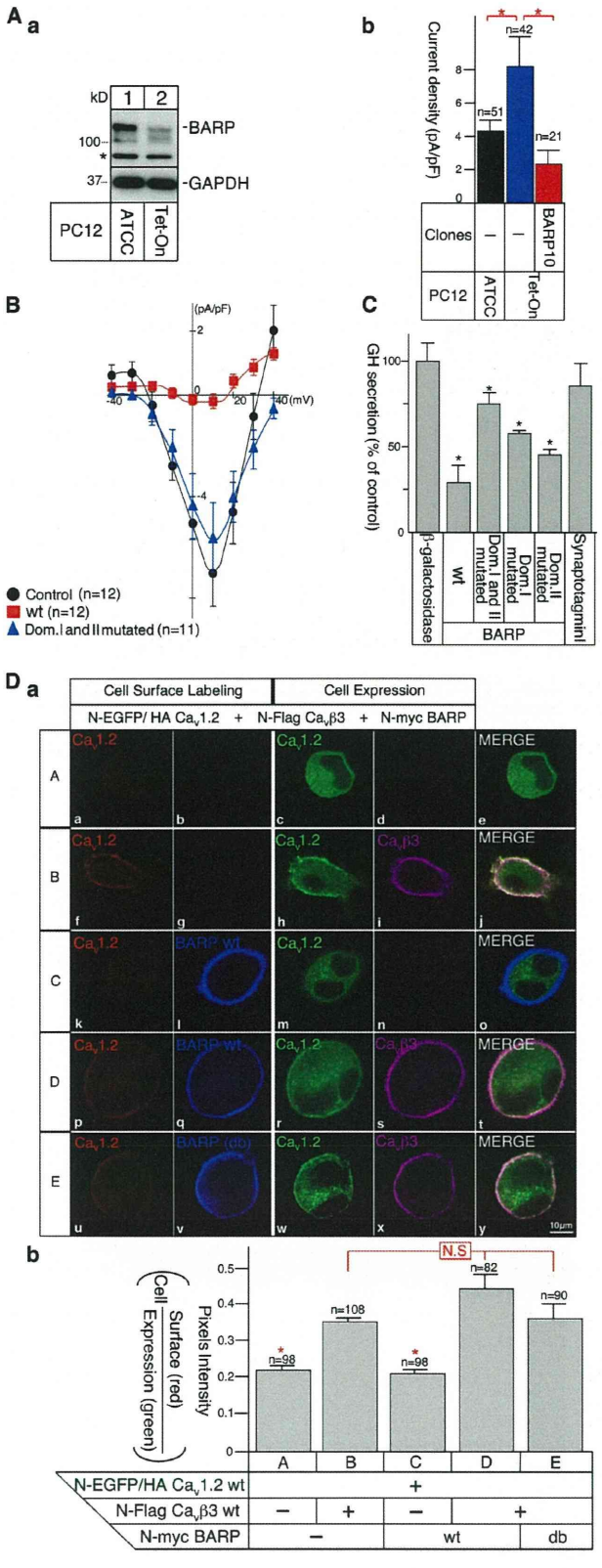

Figure 7. **BARP down-regulates VGCC activity at the plasma membrane and inhibits Ca^{2+}-dependent hormone secretion in PC12 cells.** (A) Expression of endogenous BARP in different PC12 cell lines and VGCC Ca^{+} current recordings in ATCC PC12 cells, PC12 Tet-On cells, and PC12 Tet-On cells stably overexpressing BARP (BARP10). (a) WB analysis. BARP detected in lysates from PC12 cells (ATCC) and PC12 Tet-On cells using mAb 12B1. GAPDH served as a control. The asterisk indicates the nonspecific band detected in PC12 cells. (b) Ca^{+} current recordings. Seven independent experiments were performed for each cell line, and the data were combined each to obtain the indicated *n* values. Shown are the means ± SEM for the indicated *n* values. Paired Student's *t* test. *, $P < 0.05$. (B) BARP down-regulates endogenous Ca^{2+} channel activity in PC12 cells. PC12 cells were transfected with a vector carrying WT or mutated BARP and EGFP cDNAs. Cells expressing EGFP were selected for electrophysiology. I–V relationships of Ca^{2+} channels for cells expressing the different BARP proteins are shown. Three independent experiments were performed, and the data were combined to obtain the indicated *n* values. Shown are the means ± SEM. Paired Student's *t* test at 20 mV: control versus BARP WT or domains I and II mutated ($P < 0.01$). (C) BARP inhibits Ca^{2+}-triggered growth hormone secretion in PC12 cells. PC12 cells were cotransfected with cDNAs for hGH and either β-galactosidase, synaptotagmin I, or WT or mutated BARP. hGH secretion in response to high K^{+} stimulation from cells coexpressing hGH and β-galactosidase was used as a control (100%). Shown are the means ± SEM; $n = 4$ independent experiments; unpaired Students *t* test: *, $P < 0.05$. (D) BARP does not affect cell surface expression of Ca^{2+} channels in PC12 cells. (a) Cell surface expression of N-EGFP/HA-$Ca_v1.2$ and N-Myc–BARP monitored in the presence or absence of $Ca_vβ3$ by immunofluorescence microscopy. PC12 cells were electroporated with cDNAs for N-EGFP/HA-$Ca_v1.2$ alone (A) either together with N-Flag–$Ca_vβ3$ (B) or N-Myc–BARP (C) or with Flag-$Ca_vβ3$ and WT BARP or BARP with mutated domains I and II (D and E). $Ca_v1.2$ and BARP expressed at the cell surface in nonpermeabilized cells were detected using Ab to the extracellular HA epitope in $Ca_v1.2$ and Myc in BARP. Cellular expression of EGFP-$Ca_v1.2$ and $Ca_vβ3$ are shown. Merged images are shown on the right. (b) Quantification of channel cell surface expression is expressed as the relative surface expression of HA versus EGFP-$Ca_v1.2$ (red/green). Shown are the means ± SEM. Unpaired Student's *t* test: *, $P < 0.01$. db, both domains I and II mutated; Dom., domain.

the presence of BARP was not modified, suggesting that single channel conductance, opening probability, or sensor movement rather than the kinetic or activation threshold is affected. More detailed electrophysiological studies of single channel dynamics will be required to elucidate how BARP affects VGCC activity. Although BARP does not alter surface expression of the $Ca_vα1$ subunit in tsA201 and PC12 cells, we cannot rule out an effect on VGCC trafficking in other cell types and/or under certain conditions.

One possible function of BARP could be that of an acceptor/donor for the reversible transfer of $Ca_vβ$ from/to the $Ca_vα1$ subunit. Such a reversible transfer could provide an attractive mechanism to retain the $Ca_vβ$ in the active zone to allow for the rapid modulation of VGCC activity. Thus, BARP may provide the first example of a negative modulation though the displacement of $Ca_vβ$ from the $Ca_vα1$ subunit. The presynaptic protein Rim1 also interacts with $Ca_vβ$ to anchor it to secretory vesicles (Kiyonaka et al., 2007; Gandini et al., 2011; Weiss et al., 2011), but in contrast to BARP, Rim1 stimulates Ca^{2+}-dependent secretion by preventing voltage-dependent VGCC inactivation (Kiyonaka et al., 2007).

BARP is abundant in the brain and pancreas, in which Ca^{2+}-regulated exocytosis through activation of L-type VGCC plays important roles in the release of neurotransmitters and hormones. Calcium channelopathies are congenital or noninherited muscular, neurological, and cardiac diseases associated with the gain or loss of VGCC function (Bidaud et al., 2006). Ca^{2+} channel inhibitors represent one of the most active areas of pharmacological drug development. Overexpression of BARP, or peptides encoding domains I and/or II, may be used as

Published April 21, 2014

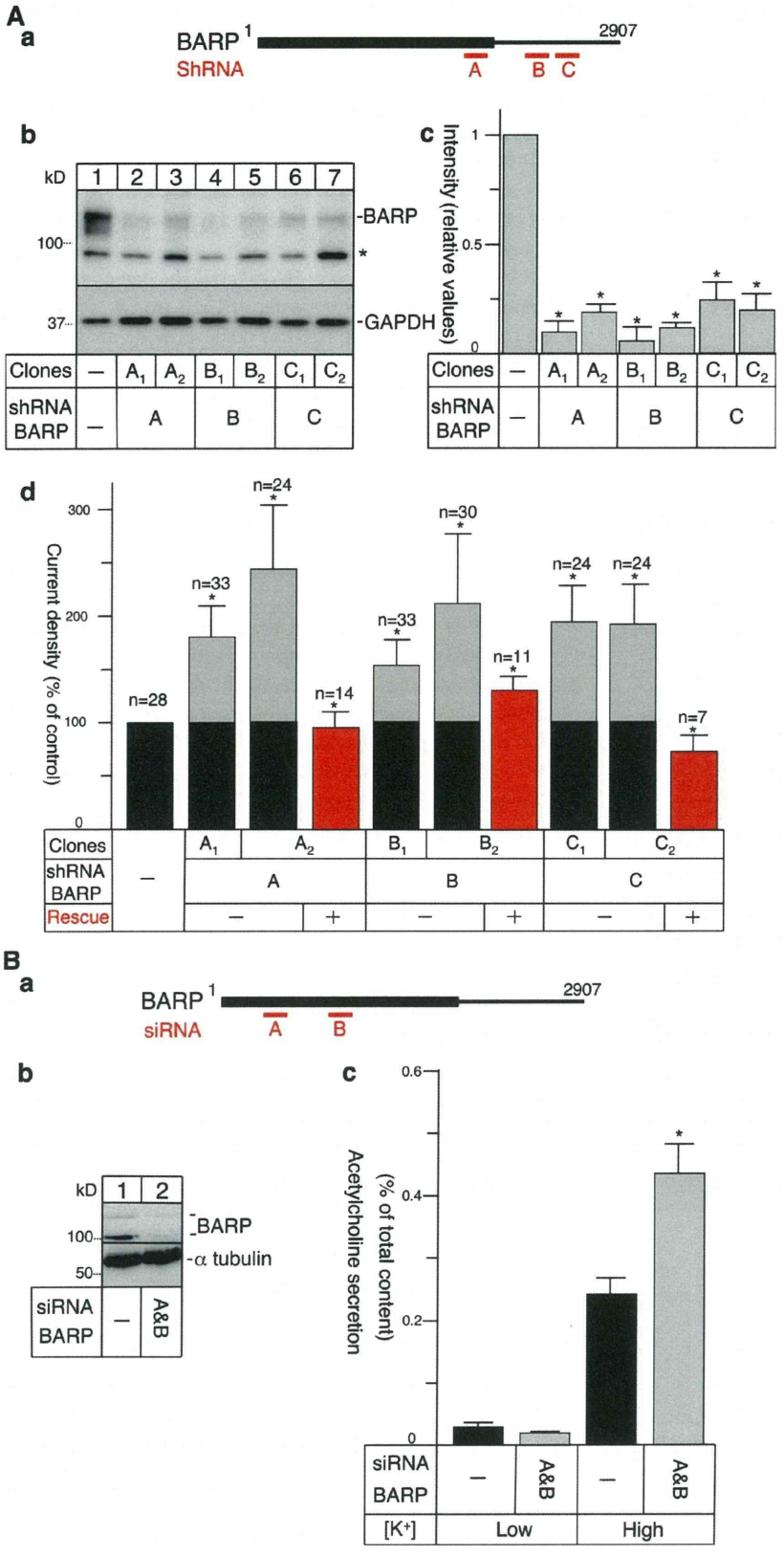

Figure 8. **Silencing of BARP enhances VGCC activity and Ca^{2+}-evoked secretion.** (A) Silencing of BARP enhances VGCC Ca^{2+} currents. (a) Schematic location of three BARP shRNA target sequences (A–C) in the rat BARP mRNA. (b) Silencing of endogenous BARP by shRNAs. WB detection of endogenous BARP and GAPDH in lysates from either ATCC PC12 control cells or cells constitutively expressing single BARP shRNAs. The asterisk shows a non-specific band detected in PC12 cells. Two clones for each shRNA were selected, and BARP (mAb 12B1) and GAPDH were detected. (c) Quantification of the efficiency of BARP shRNA knockdown. WBs were scanned, and the density values for the BARP protein bands were normalized to those of the respective GAPDH bands. The relative amount of BARP present in control PC12 cells was set to 1. Means ± SEM are shown for $n = 5$; unpaired Student's t test control versus shRNA-expressing clones: *, $P < 0.01$. (d) Ca^{2+} current density recordings in PC12 control cells and cells stably expressing BARP shRNAs. The control current was set to 100. For rescue experiments (red bars), cells expressing BARP shRNAs were transfected with a BARP mouse cDNA with a different codon usage. Means ± SEM are shown for eight (silencing) and four (rescue) experiments, and the data were combined to obtain the indicated n values; unpaired Student's t test control versus shRNA-expressing clones: *, $P < 0.05$. (B) Silencing of BARP enhances Ca^{2+}-evoked secretion. (a) Schematic location of the two BARP siRNA target sequences (A and B) in the rat sequence. (b) Silencing of endogenous BARP by siRNAs. WB detection of endogenous BARP (mAb 12B1) and α-tubulin as a control in lysates from ATCC PC12 cells or cells transfected with both siRNAs. Three independent experiments were performed, and a representative example is shown. (c) Acetylcholine secretion was determined in control and siRNA-transfected PC12 cells after low or high potassium stimulation. Shown are the means ± SEM; $n = 4$ independent experiments; unpaired Student's t test: *, $P < 0.05$.

Published April 21, 2014

Ca^{2+} channel modulators. The identification of BARP may thus open new avenues for the design of novel therapeutic VGCC blockers.

Materials and methods

Molecular biology

The yeast two-hybrid screens were performed as follows. A yeast strain L40 (*MATa trp1 leu2 his3 LYS2::lexA-HIS3 URA3::lexA-lacZ*) was transformed with a derivative of pBTM116 encompassing $Ca_v\beta3$ subunit amino acid residues 50–484 fused to the LexA DNA-binding domain. A mouse MIN6 cell cDNA library was then screened, and after histidine selection, positive clones were further confirmed to be true positives by β-galactosidase activity measurement. Eight positive clones that presented fragments of BARP cDNA were found. A BARP alanine mutagenesis scan for aa 280–485 was assessed by substituting three by three the amino acids of BARP to alanine and processed for β-galactosidase activity measurements using paper filters stained with 5-bromo-4-chloro-3-indolyl-β-D-galactopyranoside (Béguin et al., 2001). Full-length mouse BARP was isolated by conventional screening of MIN6 cDNA libraries with a partial mouse cDNA. Sequence analysis of EST clones from mouse, rat, and human (see legend of Fig. S1 A) confirmed that BARP is translated from a 3-kb transcript. Rat $Ca_v\beta1b$, $Ca_v\beta21$ (e.g., β2A), $Ca_v\beta3$, and $Ca_v1.2$ were originally cloned in S. Seino's laboratory, and the $Ca_v2.1$ and $Ca_v2.2$ cDNAs were a gift from T.W. Soong (National University of Singapore, Singapore) and T.P. Snutch (University of British Columbia, Vancouver, British Columbia, Canada). Mouse $Ca_v\beta4a$ was obtained from the I.M.A.G.E. Consortium (4501980). Epitope-tagged constructs (Flag, HA, Myc, GST, and EGFP) as well as deletion and point mutants were generated by PCR-based methods and subcloned into the pME18S vector containing an SRα promoter. The internally HA-tagged $Ca_v1.2$ has been described elsewhere (Altier et al., 2002; Béguin et al., 2006). In brief, the HA sequence was introduced in the S5-H5 loop in position 697 of rabbit $Ca_v1.2$. The amino acid sequence is defined as MQTRH-HA-MQTR (MQTR are amino acids of $Ca_v1.2$, which were duplicated, underlined is an additional amino acid, and the HA sequence is without the first methionine). Northern blot analysis was performed under standard stringency hybridization and washing conditions using mouse and human BARP cDNA probes.

Ab production

Polyclonal anti-BARP Ab 72 was custom made (BioGenes) by injecting rabbits with a BARP peptide (^{131}NEAALFEQSRK^{141}) conjugated to hemocyanin and affinity purified. A GST-BARP fusion protein (aa G125-A698) was injected into mice to generate mAb 12B1 and 8B2. Epitope mapping using truncated forms of BARP located the epitopes recognized by 8B2 and 12B1 to a region between aa 380 and 698.

Cell culture and transfection

COS-1, standard (CRL-1721), and Tet-On PC12 cells as well as BHK and tsA201 cells were grown and transiently transfected with WT or mutated cDNAs using Lipofectamine (LTX; Invitrogen) and jetPRIME (Polyplus Transfection) for biochemical and immunofluorescence experiments, respectively (Béguin et al., 2001, 2005b, 2006, 2007; Mahalakshmi et al., 2007a,b). A plasmid carrying a hygromycin resistance gene and the BARP cDNA downstream of a cytomegalovirus promoter was transfected into PC12 cells using Lipofectamine LTX. PC12 clones stably overexpressing BARP were selected and maintained in 0.2 µg/µl hygromycin. BHK cells expressing functional Ca^{2+} channels reconstituted by expression of rabbit cDNAs for the different subunits have been characterized (Mori et al., 1991; Fujita et al., 1993). Silencing of BARP in PC12 cells was achieved using the pSUPER RNAi System (Oligoengine) system and shRNAs A (5′-TTCTCAAGTCCATATACGG-3′), B (5′-TAGTGTTGATTGTCCTCCT-3′), and C (5′-CTTTGTAGCAACTGTACCT-3′) with selection and maintenance of stable clones in 400 µg/ml G418. Alternatively, PC12 cells were transiently transfected using DharmaFECT (Thermo Fisher Scientific) with siRNAs A (5′-GGAUUUCCAUCACCUCAAG-3′) and B (5′-CAUGCUGACUUCAUUCAAU-3′) designed by Thermo Fisher Scientific and used for analysis 48 h after transfection. For cell surface expression analysis, PC12 cells were electroporated (1,410 V at 30 ms) using the Neon Transfection System (Invitrogen). Primary hippocampal neurons were purchased from Cambrex and cultured according to the manufacturer's instructions. Cerebellar primary cultures were prepared as previously described (Launey et al., 2004) with substitution of B27 by the N21 supplement (Chen et al., 2008). In brief, cerebella were removed from 19-d Wistar rat fetuses, minced in Ca^{2+}/Mg^{2+}-free Hank's saline (Gibco), and digested with 0.01% trypsin (15 min at 37°C). After trituration, the suspension was plated at 5,000 cells/mm^2 on 18-mm glass coverslip (Thermo Fisher Scientific) coated with poly-L-lysine and poly-L-ornithine. Culture medium (37°C at 5% CO_2) consisted of glutamate/aspartate-free DMEM/F12 supplemented with 10 mg/ml bovine insulin, 100 mg/ml BSA, 1 mg/ml gentamycin, 200 mg/ml glutamine, 100 mg/ml human apotransferrin, 40 nM progesterone, 100 nM putrescine, 30 nM sodium selenite, 500 pg/ml triiodothyronine, 3% heat-inactivated horse serum (Gibco), and 25% of astrocyte-conditioned medium (Sumitomo Corp.), renewed by half twice a week. Cells were used at 3–4 wk. All animal experimentation was approved by the RIKEN or Institute of Molecular and Cell Biology Institutional Animal Care and Use Committees. Cells were maintained in culture for 3–4 wk before immunofluorescence microscopy experiments. Tunicamycin treatment was performed by incubating COS-1 cells immediately after transfection for 2 d with 10 µg/ml tunicamycin (Sigma-Aldrich).

Immunoprecipitation and Western blot (WB) analysis

Cell homogenates were prepared in lysis buffer (50 mM Tris-HCl, pH 7.5, 100 mM NaCl, 1 mM $MgCl_2$, and 0.5% Triton X-100) supplemented with protease inhibitors and used for coimmunoprecipitation and WB analysis as previously described (Béguin et al., 2006). For better resolution of higher molecular weight proteins, some samples were run on Tris-acetate gels (7%) according to the manufacturer's instructions (Invitrogen). Rat mAb to HA (Roche), mouse mAb to Flag (M2; Sigma-Aldrich), $Ca_v\alpha1$ (NeuroMab), GAPDH, MAP2, calbindin (EMD Millipore), synaptotagmin (Stressgen), GST (Santa Cruz Biotechnology, Inc.), $Ca_v\beta3$ (Alomone Labs), GFAP (Sigma-Aldrich), and Ab to BARP (72 and 8B2) were used. Rat cerebrum and cerebellum were manually dissociated and immediately homogenized in the same lysis buffer using 15 strokes of a glass Teflon homogenizer followed by one freeze/thaw cycle. Insoluble material was removed by centrifugation. Brain, skeletal muscle, and heart lysates were purchased from Zyagen Laboratories. At least three independent experiments were performed, and representative examples are shown.

In vitro transcription/translation

BARP was synthesized in vitro using the quick-coupled transcription/translation system (TnT; Promega) according to the manufacturer's protocol.

In vitro peptide competition

For dissociation experiments, AID (^{445}AKARGDFQKLREKQQLEEDLKGALDAATQAED^{476}) and BARP domain I (^{422}SYRDLWSLRASLELHAATASD^{442}) peptides were synthesized (Mimotopes). $Ca_v\beta3$ was pulled down from cell lysates with a GST-AID (aa A445–D476) fusion protein. After extensive washing in lysis buffer (50 mM Tris-HCl, pH 7.5, 100 mM NaCl, 1 mM $MgCl_2$, and 0.5% Triton X-100) supplemented with protease inhibitors to remove unbound $Ca_v\beta3$, increasing concentrations of peptides (30, 60, 300, and 600 nM) were added in lysis buffer. After a 4-h incubation on ice, 10% of the supernatant containing any dissociated $Ca_v\beta3$ was analyzed by SDS-PAGE and WB. In the absence of competitive peptides, the GST-AID–$Ca_v\beta3$ subunit complex remained stable over the 4-h incubation period. At least three independent experiments were performed, and representative examples are shown.

Immunocytochemistry and immunohistochemistry

N-Flag–$Ca_v\beta$ subunits and BARP or N-Myc–BARP overexpressed in PC12 and COS-1 cells were stained with mouse anti-Flag (M2; Sigma-Aldrich) and rabbit anti-BARP Ab 72 or a rabbit Ab to Myc (Sigma-Aldrich) followed by Cy3-labeled donkey anti–rabbit IgG (Jackson ImmunoResearch Laboratories, Inc.) and Alexa Fluor 488 goat anti–mouse IgG (Molecular Probes) secondary Ab as previously described (Béguin et al., 2005b). PC12, primary hippocampal, or cerebellar cells were stained with rabbit Ab to MAP2 (EMD Millipore), calbindin (EMD Millipore), and GFAP (Sigma-Aldrich), BDNF (EMD Millipore), or with mouse mAb to synaptotagmin (Stressgen). Rat brains were mechanically cut into 0.3-µm-thick sections and incubated in 10% TCA for 30 min before staining. Mouse pancreas was fixed in 4% PFA and subjected to standard ethanol/xylene processing, embedded into paraffin, cut into 0.5-µm sections, and rehydrated in graded ethanol. Slices were then washed three times with 30 mM PBS-glycine and incubated 1 h in a blocking buffer (10% goat serum, 2% BSA, and 0.4% Triton X-100), and Ab incubations were performed as described in this paragraph. For the 72 BARP Abs, antigen retrieval was achieved by incubating fixed slices for 30 min in 10 mM Tris-HCl, pH 9.0, 1 mM EDTA, and 0.05% Tween 20 at 80°C followed by three washes in PBS

Published April 21, 2014

before blocking. Antigen retrieval in pancreas sections was performed in citrate buffer (10 mM sodium citrate, pH 6, and 0.05% Tween 20) in an autoclave (Retriever 2100; Prestige Medical). Mouse mAb to glucagon (Abcam) or guinea pig Ab to insulin (Abcam) was used to stain α and β cells, respectively, in pancreatic islets. Labeled specimens were mounted in FluorSave (Vector Laboratories) or ProLong Gold (Invitrogen) and visualized using a confocal microscope (LSM 510 Meta [Carl Zeiss] or FluoView FV1000 [Olympus]). Antigen preabsorption experiments were performed by incubating GST-BARP (G125-A698) fusion protein (1 µg) linked to Sepharose beads with anti-Myc and anti-BARP Ab (72, 12B1, or 8B2) in lysis buffer for 2 h at 4°C. After a short centrifugation, the supernatant was collected and mixed with blocking buffer (1:1) before being applied to PFA-fixed cells expressing N-Myc–BARP or cerebellum slices fixed in 10% TCA.

Cell surface expression assays

To detect cell surface expression of N- or C-terminally tagged BARP or a $Ca_v1.2$ carrying a tag in an extracellular loop (Béguin et al., 2001; Altier et al., 2002), we took advantage of the fact that Abs to the tags when added to nonpermeabilized intact cells only bind and label the cells if the tag is exposed on the cell surface. Thus, intact transfected COS-1, tsA201, or BHK cells were incubated with 2 µg/ml rat anti-HA (Roche) and/or 1 µg/ml rabbit anti-Myc Ab (Sigma-Aldrich) for 1 h and then washed twice in ice-cold PBS before fixation. In some experiments, the cells were subsequently permeabilized and incubated with a different Ab to detect an intracellular protein such as the $Ca_v\beta$ subunits and EGFP-$Ca_v1.2$ in the same cells. Visualization by immunofluorescence microscopy was as described in the previous section.

Quantification of surface channel expression was performed as follows: a random 540 × 540–µm area was scanned for each coverslip at 488 nm (EGFP-$Ca_v1.2$ cell expression), 546 nm ($Ca_v1.2$ surface expression), and 633 nm (N-Myc–BARP surface expression) using a microscope (Eclipse Ti; Nikon; 20×, 1.0 NA oil objective) with a motorized stage with NIS element AR software version 4.0 (Nikon). Cells expressing $Ca_v1.2$ alone or with $Ca_v\beta3$ were first selected blindly based on EGFP fluorescence only (reflecting $Ca_v1.2$ total expression) and segmented, without looking at the surface expression. The mask thus defined was then applied to all fluorophores, and mean pixel intensity for each cell was calculated, yielding $Ca_v1.2$ total expression (488 nm) and relative surface localization (546/488 nm). Cell surface expression of $Ca_v1.2$ with $Ca_v\beta3$ together with BARP WT or domain I and II mutated was performed by first blindly selecting cells expressing BARP (633 nm), without looking at the total or surface expression of EGFP-$Ca_v1.2$. Again, the thus defined regions of interest were used as a mask to measure mean pixel intensity for each cell and each channel. To ascertain that quantification is not affected by Cav1.2 cellular expression, a cutoff corresponding to half of the mean pixel intensity of EGFP-$Ca_v1.2$ in the absence of BARP was applied.

Colocalization analysis

Fluorescence colocalization was quantified using the ImageJ/Fiji (National Institutes of Health; Schneider et al., 2012) with the plugin Coloc 2 (version December 2011), after confocal image acquisition with 62-nm/pixel spatial oversampling (FluoView FV1000 confocal with 100×, 1.4 NA oil objective, software version 4.0). For each cell, five independent optical sections were acquired at low noise (Kalman filter 5), sequentially for each channel, with negligible bleed through between channels. For accurate sampling of the different cell compartments, the five sections were projected into single images (one per channel) before background subtraction and colocalization analysis. Region of interest was defined automatically by applying a logical OR operation the two segmented channels, to select pixels that are above background in each channel. The colocalization index is reported as the thresholded Pearson's correlation coefficient, as it is more robust than other metrics (Adler and Parmryd, 2010). For each condition, at least 13–30 cells from three independent replicates were analyzed.

Electrophysiology

Whole-cell patch clamp recordings were made on BHK, PC12, and tsA201 cells using bath solution containing 40 mM Ba^{2+} at 37°C as previously described (Béguin et al., 2001, 2006). In brief, to obtain expression of EGFP and BARP, the WT or mutated BARP cDNAs were transfected into the P/Q or N type–expressing BHK cell lines or PC12 cells using the pCMS-EGFP vector (Takara Bio Inc.). Cells expressing the EGFP were selected for measurements. For expression in the tsA201 cells, WT and mutated BARP cDNA were cloned into a pCMS-EGFP vector in which EGFP had been replaced by mCherry and cotransfected with a pCMS-EGFP vector carrying the cDNAs for $Ca_v1.2$ and $Ca_v\beta3$ separated by an internal ribosomal entry site. Cells expressing EGFP and mCherry were selected for measurements. For each cell, current density (I_{Ba}) was calculated by dividing the total current by the membrane capacitance. The holding potential was −60 mV, and test pulses of 400 ms at potentials between −40 and 60 mV in steps of 10 mV were applied every 4 s. The membrane potential was measured by the perforated patch clamp method in the current clamp mode as previously described (Gonoi et al., 1994).

Growth hormone secretion and membrane potential

Secretion of transfected human growth hormone (hGH) or acetylcholine by PC12 cells were assayed as described previously (Béguin et al., 2001; Kiyonaka et al., 2007). In brief, PC12 cells were cotransfected with pXGH5 vector (Nichols Institute) containing an SRα promoter driving WT or mutated BARP, using Lipofectamine (Invitrogen) according to the manufacturer's instructions. After 3 d, PC12 cells were washed with a physiological salt solution (PSS; 140 mM NaCl, 4.7 mM KCl, 2.5 mM $CaCl_2$, 1.2 mM $MgCl_2$, 1.2 mM KH_2PO_4, 20 mM Hepes, pH 7.4, and 11 mM glucose) and incubated for 10 min with a high K^+ solution (PSS containing 60 mM KCl and 85 mM NaCl) or a low K^+ solution (PSS containing 4.7 mM KCl and 140 mM NaCl). Growth hormone was measured with a colorimetric immunoassay kit (Roche). Acetylcholine secretion in PC12 cells (Kiyonaka et al., 2007) was assayed with the similar basic procedure with the exception that pXGH5 was replaced by pEFmChAT cDNA, and acetylcholine release was measured using HPLC with electrochemical detection (HTEC-500; EiCOM).

Molecular modeling

In silico modeling, molecular dynamics, and energy refinements were performed using the Sybyl 7.2 software package (Tripos, Inc.). The $Ca_v\beta$ subunit crystal structure (Protein Data Bank accession no. 1VYT) was used as a template to dock the BARP domain I. This domain was modeled as an α helix in a reverse orientation. Amino acid W427 of BARP was positioned similarly to residue W440 of AID followed by molecular dynamics simulations (1,000 fs with 1-fs steps at 300 K) between residues of the $Ca_v\beta$ subunit and domain I within 6 Å. The lowest energy conformation was then obtained by energy minimization using Powell's method (Fletcher and Powell, 1963). The α-helical model of domain I shown in Fig. S3 D was generated using Phyre2 (Kelley and Sternberg, 2009).

Data and statistical analysis

Statistical significances were tested using unpaired and paired Student's *t* tests, and results were expressed as means ± SEM for the indicated *n* values. For coprecipitation, pull-down, WB, and immunofluorescence microscopy experiments, at least three independent experiments were performed, and a representative example is shown.

Online supplemental material

Fig. S1 shows alignment of BARP protein sequences of different species, evidence for the specificity of antibodies to BARP, and the assignment of the initiation methionine and glycosylation of BARP. Fig. S2 shows expression of BARP during mouse development, evidence for the specificity of the antibodies for immunohistochemistry localization of BARP in brain and pancreas, localization of overexpressed BARP and overexpressed synaptotagmin I, and membrane localization of $Ca_v\beta$ subunit isoforms by BARP. Fig. S3 shows the identification of domains and amino acids in BARP that mediate the interaction with $Ca_v\beta$ and molecular dynamics modeling of the interaction of BARP domain I with the ABP of $Ca_v\beta$. Fig. S4 characterizes the effect of BARP on the association of the $Ca_v\beta$ with the $Ca_v\alpha1$ subunit and the association of BARP with different $Ca_v\beta$ subunit isoforms in brain. Fig. S5 analyzes the effect of BARP on VGCC activity and surface expression and presents a working model for BARP as a $Ca_v\beta$-anchoring protein. Online supplemental material is available at http://www.jcb.org/cgi/content/full/jcb.201304101/DC1.

We gratefully acknowledge the technical support from the Support Unit for Bio-Material Analysis, Brain Science Institute Research Resources Center for DNA sequencing and cell sorting and the Institute of Molecular and Cell Biology DNA Sequencing Facility for DNA sequencing.

This work was supported by the Agency for Science, Technology and Research, Singapore and the RIKEN Brain Science Institute, Japan.

The authors declare no competing financial interests.

Submitted: 16 April 2013
Accepted: 17 March 2014